Numerical Modeling of Turbulent Combustion and Flame Spread

Yan, Zhenghua

1999

Numerical Modeling of Turbulent Combustion and Flame Spread

Zhenghua Yan

Center of Combustion Science and Technology,
and Department of Fire Safety Engineering,
Lund University, Box 118, S-22100, Lund, Sweden

Email: Zhenghua.Yan@brand.lth.se
Web page: http://www.brand.lth.se/personal/yan/yan.htm

To my wife, Yan Liu

ACKNOWLEDGEMENT

First, I would like to give my special thanks to my supervisor, Prof. Göran Holmstedt for his support, encouragement and for his letting me have my own motivation and carry out this work independently.

I also would like to deeply acknowledge Dr. John deRis (Factory Mutual Research Corporation, USA) for valuable discussions and his introducing me to the Radiation Narrow Band model, and Prof. Weicheng Fan (University of Sci. & Tech. of China) for his introducing me to the Computational Combustion during my master study in USTC.

Thanks also go to Prof. Macus Aldén, program director of the Center of Combustion Science and Technology (CECOST), and Dr. Fabian Mauss (Combustion Physics Department), for their initiating and leading the soot project, in which I have been involved. During the period of this work, I received much help from the staff of the department and CECOST, including the former secretary of the department, Maria Andersen, the Senior Lecturer of the department, Dr. Björn Karlsson and the CECOST administrative manager Jörgen Hasth. Their help has been very much appreciated.

This work was financially supported by the Swedish Fire Research Board (BRANDFORSK) and CECOST, which are gratefully acknowledged.

Last, but not the least, I express my great appreciation to my wife, Yan Liu, my parents and all the other members of the family, for their love and support.

CONTENT

1. ABSTRACT

Theoretical models have been developed to address several important aspects of numerical modeling of turbulent combustion and flame spread. The developed models include a pyrolysis model for charring and non-charring solid materials, a fast narrow band radiation property evaluation model (FASTNB) and a turbulence model for buoyant flow and flame.

In the pyrolysis model, a completely new algorithm has been proposed, where a moving dual mesh concept was developed and implemented. With this new concept, it provides proper spatial resolution for both temperature and density and automatically considers the regression of the surface of the non-charring solid material during its pyrolysis. It is simple, very efficient and applicable to both charring and non-charring materials.

FASTNB speeds up significantly the evaluation of narrow band spectral radiation properties and thus provides a potential of applying narrow band model in numerical simulations of practical turbulent combustion.

The turbulence model was developed to improve the consideration of buoyancy effect on turbulence and turbulent transport. It was found to be simple, promising and numerically stable. It has been tested against both plane and axisymmetric thermal plumes and an axisymmetric buoyant diffusion flame. When compared with the widely used standard buoyancy-modified $k-\varepsilon$ model, it gives significant improvement on numerical results.

These developed models have been fully incorporated into CFD (Computational Fluid Dynamics) code and coupled with other CFD sub-models, including the DT (Discrete Transfer) radiation model, EDC (Eddy Dissipation Concept) combustion model, flamelet combustion model, various soot models and transpired wall function. Comprehensive numerical simulations have been carried out to study soot formation and oxidation in turbulent buoyant diffusion flames, flame heat transfer and flame spread in fires. The gas temperature and velocity, soot volume fraction, wall surface temperature, char depth, radiation and convection heat fluxes, and heat release rate were calculated and compared with experimental measurements.

In addition, to provide comprehensive data for comparison, experiments on room corner fire growth were undertaken, where the gas temperature, solid fuel surface temperature, radiative heat flux, char depth and heat release rate were all measured.

2. INTRODUCTION

Combustion and its control are of great importance in many industrial applications and environment protection. A large amount of power and heat is produced by combustion of hydrocarbon fuels and a heavy effort in combustion research is now placed on the control and reduction of pollutant emission. Fire is an unwanted combustion, which deteriorates environment and causes great loss of life and property. Combustion in both industrial applications and fires share many basic aspects, but also hold their own distinguishing features. Combustion in fires is normally a buoyancy-controlled natural burning of complex fuels in large and complex geometries, with energy intensity of about 1 MW/m^3, which is low compared to that of 100-1000 MW/m^3 in industrial applications [1].

One of the main purposes of studying combustion in fires is to understand better how the combustion proceeds and how the flame spreads. Flame spread in fires is the flame propagation over solid or liquid fuel surface. It indicates fire growth with the involvement of more and more fuels. In combustion, chemical energy is released as heat. The solid and/or liquid materials around the combustion source can be heated up through both convection and radiation heat transfer. If the material is combustible, when sufficiently heated up, it will start to evaporate and/or pyrolyse to release gas fuels. The released gas fuels will likely be ignited. As a result, flame spreads over and combustion grows.

Combustion in practice is usually very complex, with a large number of strongly interactive sub-processes involved, including chemical reactions, turbulent flow and radiative heat transfer, etc. Many sub-processes are highly complex themselves. The reaction mechanism of many practical fuels is far from being fully understood. Turbulence remains an unsolved difficult problem after much dedicated study. Although the radiation study benefits from quantum mechanics theory and bears a better understanding in principle, an exact solution of thermal radiation in a practical combustion system is impossible. In combustion of solid fuels, the complex physical and chemical processes inside solid fuels and the interaction between gas and solid phases impose extra difficulty.

The mathematical description of a practical turbulent combustion process turns out to be highly non-linear and time and space dependent. Therefore, theoretical modeling and simulation of turbulent combustion is now mostly based on numerical solution, resorting to computers to resolve the mathematical complexities. Different extents of computer resorting result in different solution strategies. In principle, an established mathematical description can directly be solved using a solution method termed Direct Numerical Simulation (DNS). However, in turbulent combustion, there is a wide range of related time and space scales, which may differ by several orders of magnitude. In order to implement DNS, one has to resolve the smallest scales properly, in both space and time coordinates. This resolution turns out to be very computer resource demanding [2] and thus creates resolution problem for direct simulation of practical combustion processes. To overcome the resolution problem, one commonly used method is the Reynolds Averaged Simulation (RAS), where the instantaneous equations are statistically averaged for solution and thus only the relatively smooth mean field needs to be resolved properly. The contribution of fluctuation to the averaged values is modeled using models. Another method is the so-called Large Eddy Simulation (LES). In LES,

eddies down to the inertial range are resolved properly. The contribution of smaller eddies is modeled using sub-grid modeling. Since the small eddies are not tuned at the same range of frequency of the mean flow, sub-grid modeling can be expected to be relatively more universal. Although the computer resource demand of LES is much less than that of DNS, it is still not practical in many engineering combustion simulations, particularly when radiation is to be properly considered.

The involvement of radiation in combustion makes the numerical simulation even further computer resource demanding. Radiation is usually an important heat transfer mechanism in combustion. It is proportional to the black body Planck function and the emissivity of the participating medium, which increases with the radiating path length and the absorption coefficient of the medium. Radiation heat transfer differs from convection in many aspects. Transfer of a radiated photon does not need the support of any medium. It has strong direction and wave number dependence in most practical situations, such as those in a combustion system where the radiating gas is highly non-gray and non-homogeneous. Thus, radiation essentially has seven independent variables, i.e., $I = I(\vec{r}, \vec{s}, \eta, t)$, where I is the directional spectral radiation intensity, $\vec{r}$ the location vector in a three dimensional space, $\vec{s}$ the direction vector of two independent variables, η the wave number and t the time. This complexity implies that an exact solution of radiation in a practical combustion system is not available and numerical computation of radiation can be very expensive.

When solid fuel is presented in the combustion system, consideration also has to be given to the response of the solid fuel and the interaction between gas and solid phases. The solid fuel may undergo a series of complex physical and chemical processes differently according to the local conditions. The interaction includes the mass, energy and momentum exchanges between the two phases. When the solid fuel is in the small particle form, this interaction is particularly complex and thus an important topic in two-phase studies.

To meet the needs in combustion engineering applications, models are developed and implemented, to represent the physics approximately and speed up the numerical computations to an acceptable level, with a proper compromise made between accuracy and economy. A good model should provide both high accuracy and efficiency in a wide range of applications.

In this work, models on pyrolysis of solid fuels, radiation property of combustion products and turbulence of buoyant flow were developed, with emphasis on their applicability and simplicity. These developed models have been fully incorporated into CFD and coupled with other CFD sub-models, including DT radiation model, EDC combustion model, flamelet combustion model, various soot models and transpired wall function. Comprehensive numerical simulations have been carried out to study soot formation and oxidation in turbulent buoyant diffusion flames, flame heat transfer and flame spread. The gas temperature and velocity, soot volume fraction, wall surface temperature, char depth, radiation and convection heat fluxes, and heat release rate were calculated and compared with experimental measurements.

3. THEORETICAL MODELS

A numerical simulation of flame spread over solid fuel surface consists of modeling of three main parts: turbulent combustion, response of solid fuel and the interaction between gas and solid phases. The first two parts will be discussed in this section. The third part provides the necessary boundary conditions for the other two parts and will be discussed later in the boundary condition section.

3.1 Modeling of Turbulent Combustion

In this section, some physics of turbulence and turbulent combustion will be discussed first, then the used modeling procedure presented.

3.1.1 Some basic physical aspects of turbulence and turbulent combustion

Turbulence remains one of the most challenge topics nowadays. It can be considered as a deterministic random hydrodynamic system. It is deterministic in a sense that provided a unique set of initial and boundary conditions, it is believed to hold a unique solution. It is random in a sense that when the Reynolds number of the flow is sufficiently high, the system becomes unstable. The flow solution in this case turns out to be very sensitive to the external disturbances including the initial and boundary conditions.

Although it is very difficult to give an exact definition of turbulence, its general main features can be identified [3]. The irregularity is one of the most important features of turbulence, which is in contrast to the regularity of laminar flow. The random motion of turbulence enhances the mixing process sharply and turbulence is thus diffusive. Turbulence comes from the instability of the viscous flow at high Reynolds number, which results from the interaction between the viscous and non-linear inertial terms of the Navier-Stokes equations. The interaction is very complex and makes it a prohibitive task to fully analyse the flow instability. Turbulence holds a continuous spectrum of scales ranging from integral scales to Kolmogorov scales. It obtains its kinetic energy from mean flow through shear and buoyant production. The large eddies which have comparable dimension of mean flow gain most of the energy and thus are the energy containing eddies. The kinetic energy will largely be transferred to smaller eddies when the smaller eddies are stretched by the larger eddies. Most of the turbulence kinetic energy will be dissipated at the smallest eddies. Therefore, turbulence is always dissipative. At the inertial range of eddies, if we ignore the small dissipation, the energy received from larger eddies is equally transferred to smaller eddies. This gives the picture of the turbulence kinetic energy cascade. Figure 1 shows an illustrative spectral energy transfer function which describes the net energy transfer among eddies [4]. The rotational nature of turbulence and the turbulence maintaining mechanism of vortex stretching bring turbulence to a three-dimensional space, since vortex stretching does not exist in a two-dimensional space. The dissipation character of turbulence is closely related to that of rotational. The rotation of the flow favors the creating of many regions of large gradients, thus enhances the dissipation.

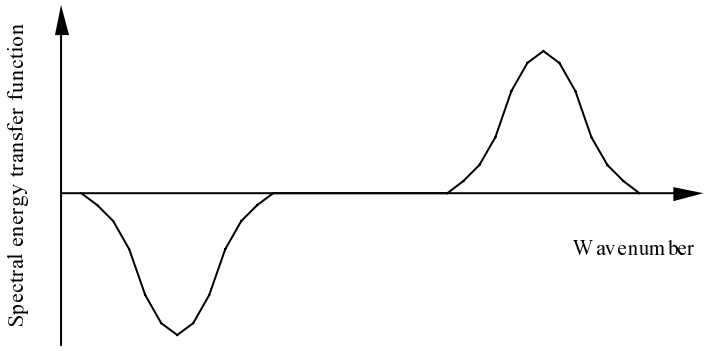

Fig. 1 Illustrative spectral energy transfer function

The present of combustion in a turbulent flow complicates the problem further. Unfortunately, combustion in practical applications almost always finds itself accompanied by turbulence. There is a strong interaction between combustion and turbulence. Both of them have dual effects on each other. The heat released by combustion will cause the thermal expansion of the fluid mixture, thus drive a flow. The viscous flow may loose its stability when the Reynolds number of the flow is sufficiently high and the transition from laminar flow to turbulent flow may happen. On the other hand, the reduction of the fluid density has a damping effect on vorticity, thus may damp turbulence. Meanwhile, turbulence also has dual effects on combustion. In a diffusion flame, the fuel and oxidant need to be mixed at molecule level first before the reaction can happen. In a premixed flame, the flame propagation depends on the heat conduction and radical diffusion from burned region to unburned region. Many chemical reactions have much smaller time scales than the physical mixing process. Thus the mixing is often crucial for combustion and the turbulent combustion often turns out to be mixing controlled in many senses. As a result, the turbulence, which can enhance mixing, may intensify combustion, in both diffusion and premixed flames. However, strong turbulence may also affect the flame structure and increase flame heat loss rate to an extent that the flame may be extinguished by the high strain rate [5-7].

Both turbulence and chemical reactions have a wide range of scales. The turbulence eddy size can range from the integral length scale to the Kolmogorov length scale. The integral length scale is of the same order of the physical dimension of the considered problem. The Kolmogorov length scale is the length scale of the smallest eddies in a turbulent flow. According to the Kolmogorov's theory [3, 8, 9], it can be estimated as $(\nu^3/\varepsilon)^{1/4}$, where ν is the kinematic viscosity and ε is the dissipation rate of turbulence kinetic energy. The Kolmogorov length scale can be as small as 0.1 mm. Turbulence time scales vary from the integral time scale of the large eddies to the Kolmogorov time scale of the smallest eddies. The integral time scale is of the order of l/u', where l is the integral length and u' is the rms value of velocity fluctuation. The Kolmogorov time scale can be estimated as $(\nu/\varepsilon)^{1/2}$, where the turbulence kinetic energy dissipation rate ε can be estimated as $(u')^2/(l/u') = (u')^3/l$. The ratio of the integral time scale to the Kolmogorov time scale is the square root of the Reynolds

number, which is usually quite large. In chemical reactions, the time scale can also vary by several orders of magnitude, going from the fast heat release reactions to the slow pollution formation reactions such as the NO_x and soot formation.

Depending on the relation between these scales, turbulent combustion can fall into several distinguished regimes. The ratios of the corresponding flow scales and chemical scales define several non-dimensional numbers, including Reynolds number, Damköhler number and Karlovitz number. These numbers have their clear physical interpretation and thus give some indication on the status of the combustion. Borghi's diagram gives a good conceptual description on this point for a premixed flame. See [7, 10, 11] for details.

Assuming the time dependent Navier-Stokes equations contain all the physics of a turbulent flow and we have all the knowledge of the concerned chemistry, a direct numerical solution for a turbulent reacting flow can be obtained in principle. However, in the direct simulation, all the relevant scales should be sufficiently resolved. As mentioned before, this will cause resolution problems, since there exists a wide range of scales and the smallest scales are usually very small. Fortunately, the most concerned is the mean property in most practical engineering applications. Mean property is relatively smooth in both time and space coordinates, thus allows us to overcome the resolution difficulty. However, we have to keep in mind that the fluctuation has a significant influence on the mean field. As a result, when seeking the averaged solution, the resolution difficulty is switched to the closure problem, which has to be solved, by modeling, for example.

Accurate modeling of turbulent combustion requires a proper consideration of all the important physics and chemistry. The physical aspects briefly discussed above give some important clues for the modeling strategy and possible simplifications. In the turbulence modeling, the spectrum of the turbulence scales explains why the conventional turbulence modeling cannot be universally applicable. The length and time scales of large eddies are comparable to those of mean flow. As a result, turbulence is a property of the flow. Any conventional turbulence model, which is tuned for certain types of flow, may fail in other situations. In LES, since the modeled small eddies do not have strong direct interaction with the mean flow, the LES modeling can be expected to be more universal. Concerning the combustion modeling, when the time scale of the concerned chemistry is much smaller than that of mixing, the combustion is mixing controlled and one may reasonably assume that combustion happens once the fuel and oxidant is mixed and activated. The mixing control assumption allows the combustion analysis to be significantly simplified. This is the starting point of the Magnussen's EDC combustion model [12, 13] which will be discussed later. The fast chemistry assumption is also one of the key points in the development of the flamelet combustion model [14-20], where the turbulent flame is considered to be an ensemble of wrinkled laminar flamelets which have a well-defined structure.

In this thesis, the RAS method was employed to solve for the mean property, with turbulence and turbulent combustion models adopted to overcome the closure difficulty met in averaging the non-linear partial differential equations, by relating higher to lower moments. The details of the employed modeling procedure is below.

3.1.2 Governing equations

The classical description of a combustion problem is based on continuum mechanics, assuming local mechanic and thermal equilibrium, and local chemical homogeneity. The governing equations of instantaneous properties can be derived from kinetic theory based on the conservation law. See [21, 22] and the references cited there for details of the equation derivation.

Using the RAS method, the governing equations of instantaneous properties are statistically averaged and the numerical computation of turbulent reacting flow is then based on the solution of a set of statistically averaged partial differential equations, comprising continuity, momentum, energy and species equations. The radiation equation and the thermal state relations provide the necessary auxiliary equations.

The flows considered in this thesis were driven by the buoyancy generated by the heat released by combustion. The maximum velocity is of the order of several meters per second (Mach number << 1.0), and the pressure variation is small, so that the effects of fluid kinetic energy and pressure variation can be neglected in the energy equation. Since there is a strong variation of density during combustion, a density weighted averaging (Favre-averaging) procedure is adopted. Ignoring the bulk viscosity, Dufour and Soret effects, the Favre-averaged equations can be written as

$$\frac{\partial \overline{\rho}}{\partial t} + \frac{\partial (\overline{\rho} \widetilde{u_i})}{\partial x_i} = 0 \tag{1}$$

$$\frac{\partial (\overline{\rho} \widetilde{u_i})}{\partial t} + \frac{\partial (\overline{\rho} \widetilde{u_i} \widetilde{u_j})}{\partial x_j} = -\frac{\partial \overline{p}}{\partial x_i} + \frac{\partial}{\partial x_j}\left[\mu \left(\frac{\partial \widetilde{u_i}}{\partial x_j} + \frac{\partial \widetilde{u_j}}{\partial x_i} \right) - \overline{\rho} \overline{u_i'' u_j''} \right] + \overline{\rho} a_{gi}$$

$$= -\frac{\partial \overline{p^*}}{\partial x_i} + \frac{\partial}{\partial x_j}\left[\mu \left(\frac{\partial \widetilde{u_i}}{\partial x_j} + \frac{\partial \widetilde{u_j}}{\partial x_i} \right) - \overline{\rho} \overline{u_i'' u_j''} \right] + (\overline{\rho} - \rho_\infty) a_{gi} \tag{2}$$

$$\frac{\partial (\overline{\rho} \widetilde{h})}{\partial t} + \frac{\partial (\overline{\rho} \widetilde{u_j} \widetilde{h})}{\partial x_j} = \frac{\partial}{\partial x_j}\left(\frac{\mu}{P_r} \frac{\partial \widetilde{h}}{\partial x_j} - \overline{\rho} \overline{u_j'' h''} \right) + \overline{S}_h \tag{3}$$

$$\frac{\partial (\overline{\rho} \widetilde{Y_i})}{\partial t} + \frac{\partial (\overline{\rho} \widetilde{u_j} \widetilde{Y_i})}{\partial x_j} = \frac{\partial}{\partial x_j}\left(\frac{\mu}{S_c} \frac{\partial \widetilde{Y_i}}{\partial x_j} - \overline{\rho} \overline{u_j'' Y_i''} \right) + \overline{R}_i \tag{4}$$

where $\overline{p^*} = \overline{p} - p_\infty + \rho_\infty a_{gi} x_i$, and is the pressure less its hydrostatic value, a_{gi} is the gravity acceleration vector, $\overline{S}_h$ is the energy source term resulting from the radiation, and

$$h = \sum Y_i h_i = \sum Y_i \left(h_{0,i} + \int_{T_0}^{T} c_{p,i}\, dT \right) \tag{5}$$

in which $h_{0,i}$ is the heat of formation of species i at temperature T_0.

Since the chemical reaction will not change the total enthalpy in a system, by solving the conservation equation for the total enthalpy, the chemical heat release does not need to be considered explicitly in the energy equation.

The gas properties, such as the dynamics viscosity μ and the heat capacity c_p, are normally strong functions of temperature, which varies widely in a combustion system. Their variations are represented by polynomial fitting, using the data from [23]. The property of the mixture is then calculated using the individual species' mass fraction as weight function.

The second moments arising from the averaging of the Navier-Stokes equation represent the contribution of the filtered out fluctuation to the averaged quantities. They need to be modeled before the averaged equations can be solved. The modeling of these second moments will be discussed later in the section of turbulence model.

Due to the non-linearity of the chemical reaction rate, the mean reaction rate can not be fully provided by the mean gas properties, such as mean mass concentrations and temperature. The fluctuations are obviously needed. This imposes an additional closure problem, which will be discussed in the combustion model section.

Since the radiation is also highly nonlinear, the consideration of the influence of turbulent fluctuation on radiation is clearly desirable. However, this requires the statistics of the mixture's thermal state and will greatly increase the computational complexity. Moreover, it was found in some earlier radiation studies [24, 25] that radiation based on mean scalars is in close agreement with measurements and the influence of turbulent fluctuation on radiation is comparable to the uncertainty in flame structure. For simplicity, the radiation was computed approximately using mean scalars.

3.1.3 Turbulence models

The closure problem in the turbulence modeling can be addressed by constructing turbulence models, which are used to somehow feed back the contribution of the filtered out fluctuation to the mean field. Many different turbulence models, of varying complexities and applicabilities, have been proposed [26], such as the mixing length model, the $k-\varepsilon$ model, the $k-\omega$ model, the Algebraic Stress Model (ASM) and the Reynolds Stress Model (RSM). Consideration should be given to both applicability and simplicity when selecting a specific turbulence model for application. Due to the complexity, the closure is often constructed heavily based on dimensional arguments, with the closure 'constants' (if there is any) derived from the relatively well defined flows. The lack of full physics prevents the closure to be universal. As a result, a model or closure, which is applicable to certain types of flow, may fail when applied to other types of flow. The confidence of applying a turbulence model to a specific type of flow can only be obtained through extensive validation and testing. In particular, a turbulence model should be used with care when it is applied to a flow with a condition under which the closure assumption introduced in the model development can be seriously violated. When applying a turbulence model, the simplicity and numerical stability of the turbulence model is also highly concerned, since the modeling is based on numerical computation. Therefore, the choice

of turbulence model mainly depends on the modeling interests and the compromise between accuracy and simplicity.

3.1.3.1 The standard $k-\varepsilon$ model

The standard $k-\varepsilon$ model is perhaps one of the most widely used model. Like all the other turbulence models, it has its own serious defects, such as limited applicability to flow of strong streamline curvature or strong rotation [26]. The defects of the standard $k-\varepsilon$ model originate from the closure assumptions including the adopted Boussinesq assumption which assumes a linear relation between the Reynolds stress and the mean strain rate. The Boussinesq assumption may fail when the flow is subject to a sudden change of strain rate or a strong rotation. When the scalar transport is involved, the simple gradient modeling procedure is normally adopted for the scalar fluxes within the framework of the standard $k-\varepsilon$ model. This introduces additional defects and leaves space for improvement. However, the standard $k-\varepsilon$ model has its important advantages that it is simple, numerically stable and has been proved successful in many practical applications. Strategies are suggested to abandon the Boussinesq assumption, for example, by constructing a non-linear relation between Reynolds stress and the mean strain rate, solving algebraic Reynolds stress equations or differential Reynolds stress equations. However, all of these alternatives have their own deficiencies, with regarding to their complexities and modeling uncertainties, for example, in the RSM, up to seven additional differential equations need to be solved and the modeling of the pressure strain redistribution term is still a challenge. Therefore, the standard $k-\varepsilon$ model remains attractive.

When applied to buoyant flows, the standard $k-\varepsilon$ model needs to be modified to include the important buoyancy effect on turbulence and turbulent transport. In this $k-\varepsilon$ modeling, two additional turbulence quantity equations are solved

$$\frac{\partial(\overline{\rho}k)}{\partial t}+\frac{\partial(\overline{\rho}\widetilde{u}_j k)}{\partial x_j}=\frac{\partial}{\partial x_j}\left(\frac{\mu_t}{\sigma_k}\frac{\partial k}{\partial x_j}\right)+\overline{\rho}(P+G-\varepsilon) \tag{6}$$

$$\frac{\partial(\overline{\rho}\varepsilon)}{\partial t}+\frac{\partial(\overline{\rho}\widetilde{u}_j \varepsilon)}{\partial x_j}=\frac{\partial}{\partial x_j}\left(\frac{\mu_t}{\sigma_\varepsilon}\frac{\partial \varepsilon}{\partial x_j}\right)+c_{1\varepsilon}\overline{\rho}\frac{\varepsilon}{k}(P+G)(1+c_{3\varepsilon}R'_f)-c_{2\varepsilon}\overline{\rho}\frac{\varepsilon^2}{k} \tag{7}$$

where $P=-\overline{u''_i u''_j}\frac{\partial \widetilde{u}_i}{\partial x_j}$ and is modeled as $P=\upsilon_t\left(\frac{\partial \widetilde{u}_i}{\partial x_j}+\frac{\partial \widetilde{u}_j}{\partial x_i}\right)\frac{\partial \widetilde{u}_i}{\partial x_j}$, R'_f is the modified flux Richardson number, $G=-\beta\overline{u''_i T''}a_{gi}$ and is modeled as $G=\beta\frac{\upsilon_t}{\sigma_t}\frac{\partial \widetilde{T}}{\partial x_i}a_{gi}$, β is the thermal expansion coefficient $-\frac{1}{\overline{\rho}}\frac{\partial \overline{\rho}}{\partial \widetilde{T}}$.

It should be noted that in the Favre-averaging, $\overline{\rho u''_i}$ is exactly zero. The buoyancy production term G in the k ($\frac{1}{2\bar{\rho}}\overline{\rho u''_i u''_i}$) equation comes from the modeling of $\overline{u''_i \frac{\partial p}{\partial x_i}}$.

The exact turbulence kinetic energy equation can be given by

$$\frac{\partial(\bar{\rho}k)}{\partial t}+\frac{\partial(\bar{\rho}\tilde{u}_j k)}{\partial x_j}=\overline{u''_i \frac{\partial \tau_{ij}}{\partial x_j}}-\overline{\rho u''_i u''_j}\frac{\partial \tilde{u}_i}{\partial x_j}-\frac{\partial}{\partial x_j}\overline{\rho u''_j \frac{1}{2}u''_i u''_i}-\overline{u''_j \frac{\partial p}{\partial x_j}} \tag{8}$$

where the pressure work term $\overline{u''_j \frac{\partial p}{\partial x_j}}$ can be rewritten as

$$\overline{u''_j \frac{\partial p}{\partial x_j}}=\overline{u''_j \frac{\partial(\bar{p}+p')}{\partial x_j}}=\overline{u''_j \frac{\partial \bar{p}}{\partial x_j}+u''_j \frac{\partial p'}{\partial x_j}}=\overline{u''_j}\frac{\partial \bar{p}}{\partial x_j}+\overline{\frac{\partial(u''_j p')}{\partial x_j}-p'\frac{\partial u''_j}{\partial x_j}}$$

$$=\overline{u''_j}\frac{\partial \bar{p}}{\partial x_j}+\frac{\partial}{\partial x_j}\overline{u''_j p'}-\overline{p'\frac{\partial u''_j}{\partial x_j}} \tag{9}$$

The first term in the above equation can be rearranged to yield

$$\overline{u''_j}\frac{\partial \bar{p}}{\partial x_j}=\overline{u''_j}\frac{\partial\overline{(p^*+p_\infty-\rho_\infty a_{gi}x_i)}}{\partial x_j}=-\frac{\overline{\rho' u'_j}}{\bar{\rho}}\left(\frac{\partial \overline{p^*}}{\partial x_j}-\rho_\infty a_{gj}\right) \tag{10}$$

where the buoyancy production term is recovered and can be written as $\overline{\rho' u'_j}a_{gj}$ if $\frac{\partial \overline{p^*}}{\partial x_j}-\rho_\infty a_{gj}=-\bar{\rho}a_{gj}$.

Due to the lack of definitive experimental data to guide the modeling, the pressure diffusion term is normally incorporated into the turbulent transport term using gradient modeling. For incompressible simple flows, the DNS data of Mansour et al [27] has shown that this term is small. The pressure strain correlation is usually ignored, although Librovich et al [28] indicated that this term could be a source for turbulence in combustion. Currently, there is still much uncertainty in the modeling of the pressure fluctuation related terms [29].

The solution of the PDEs for turbulence kinetic energy and its dissipation rate provides an estimate of the rms value of the velocity fluctuation, u, and a characteristic turbulence length scale, l, as: $u \sim k^{0.5}$ and $l \sim k^{1.5}/\varepsilon$. With the dimensional arguments and an analogy to molecule mixing, they can be used to compute the eddy viscosity $\mu_t \sim \rho u l$, which is used in the Boussinesq approximation

to model the Reynolds stress tensor $-\overline{\rho}\widetilde{u''_i u''_j} = \mu_t\left(\frac{\partial \widetilde{u}_i}{\partial x_j}+\frac{\partial \widetilde{u}_j}{\partial x_i}\right)-\frac{2}{3}\overline{\rho}k\delta_{ij}$. This provides the closure for the averaged momentum equation (Eq. 2). The scalar fluxes $-\overline{\rho}\widetilde{u''_j Y_i''}$ and $-\overline{\rho}\widetilde{u''_j h''}$ in Eqs. 3 and 4 are similarly modeled by using the simple gradient modeling method with turbulent Prandtl/Schmidt numbers introduced. This procedure provides part of the necessary closure for the set of the mean governing equations, which describe the turbulent reacting flow, leaving the mean chemical reaction rate and mean radiation source terms still to be modeled.

The modeling procedure in the above standard buoyancy-modified $k-\varepsilon$ model is simple, but has been found inadequate for the modeling of buoyant turbulent flow. It cannot capture counter gradient diffusion and tends to significantly under-predict the spreading rate of vertical thermal plume [30, 31] and over-predict the spreading rate of horizontal, stably-stratified flow [32]. Counter gradient diffusion is an important point which should be considered in the modeling of buoyancy driven turbulent flow. The heated gas has smaller density, thus can be preferentially accelerated by pressure difference, and consequently may result in counter gradient diffusion [33]. The incorrect prediction of the spreading rates can bring serious deficiencies to the prediction of the important velocity and scalar profiles.

3.1.3.2 A modified $k-\varepsilon$ model

A modified $k-\varepsilon$ two-equation turbulence model was developed in this work, with the buoyancy effect considered more properly. It was found to be stable, computationally economic, promising and applicable to complex situations. It is capable of capturing counter gradient diffusion and well predicts the plume spreading rates and velocity and temperature profiles. When compared with the standard buoyancy-modified $k-\varepsilon$ turbulence model, this model gives significantly improved numerical results, as illustrated in Fig 2. The details of the model development and the modeling of the second moments can be found in paper 5 of this thesis.

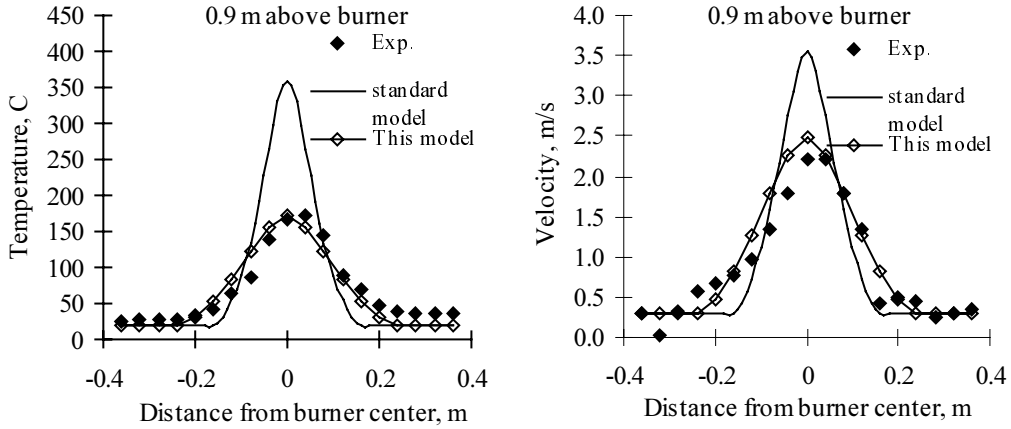

Fig. 2 Comparison of predicted and measured temperature and velocity profiles at 90 cm above a buoyant C3H6 diffusion flame

3.1.4 Combustion models

Combustion models are adopted to cope with the closure problem created by averaging the non-linear reaction rates. Two basic strategies can be employed. One is to solve the transport equations of the mean non-conserved mass fractions with the mean chemical reaction rates directly modeled. Another one is to solve the transport equation of a conserved scalar and then relate the concerned mean non-conserved mass fractions to the conserved scalar using the laminar flamelet concept and a probability density function. They are briefly discussed below.

3.1.4.1 Eddy dissipation concept (EDC)

The Eddy Dissipation Concept proposed by Magnussen and Hjertager [12] is a popular representative method to model the mean reaction rate directly. It gains its popularity since it is simple and widely applicable.

In a diffusion flame, the fuel and oxidant need to be mixed at molecule level before a reaction can happen. In a premixed flame, the flame propagation is dependent on the mixing of hot products with the unburnt mixture and the diffusion of radicals. The chemical kinetics determines how the reaction will proceed in the mixture. Therefore, combustion depends on both mixing and chemical kinetics in general, but can be essentially controlled by the slower of these two sequential processes, particularly when the slower process is much slower than the faster one. When the chemistry is much faster than the mixing, combustion turns out to be mixing-controlled. In this case, the mixing rate can well represent the combustion rate. This point is of great value in the modeling of turbulent combustion.

The mixing process in a turbulent flow is largely dependent on the property of the turbulence. In a turbulent flow, there exists a kinetic energy cascade, which was discussed earlier. The turbulence kinetic energy is extracted by the large eddies from the mean flow and dissipated mostly at the smallest eddies through molecular viscous dissipation. Therefore, the turbulence kinetic energy dissipation rate is closely related to the molecule mixing. The ratio of turbulence kinetic energy and its dissipation rate, k/ε, indicates a dissipation time scale. By dimensional argument, we may estimate the dissipation rate of a general variable φ as $c_\varphi \frac{\widetilde{\varphi}_*\varepsilon}{k}$, where $\varphi_* = \varphi''^2$ and c_φ is an empirical proportion coefficient.

Based on these arguments, the mean combustion rate can be estimated as $c_\varphi \rho \frac{(\widetilde{\varphi}_*)^{0.5}\varepsilon}{k}$, with φ representing the mass fraction. Assuming the fluctuation is simply related to the mean value, the mean reaction rate is modeled in EDC [12] by the turbulence dissipation rates of reactant and/or product eddies as

$$R_f = -\rho \frac{\varepsilon}{\kappa} \min(c_r \overline{Y}_{f,}\, c_r \frac{\overline{Y}_{ox}}{s}) \tag{11}$$

or

$$R_f = -\rho \frac{\varepsilon}{\kappa} \min(c_r \overline{Y}_{f,}\, c_r \frac{\overline{Y}_{ox}}{s},\, c_p \frac{\overline{Y}_p}{1+s}) \tag{12}$$

where the subscripts r, f, ox and p in the above equations denotes reactants, fuel, oxidant and products, respectively.

Obviously, the applicability of the above modeling procedure is limited by the introduced assumptions, especially by the fast chemistry assumption. EDC was later extended [13] for possible inclusion of chemical kinetics, after introducing a series of assumptions.

3.1.4.2 Flamelet combustion model

Due to the limited concern, the discussion of flamelet combustion model will be for non-premixed combustion only.

The main structure of laminar diffusion flame was found from measurements to be quite universal when it is plotted against the local equivalence ratio [34]. Assuming an infinitely fast chemistry, it can be shown that there exists a unique relation between mass fractions and mixture fraction for a two-stream system with equal mass diffusivities. When the chemistry is fast, but not infinitely fast, as it is in many practical considerations, to leading order, the flame structure can still be regarded as well defined on a conserved scalar space, which is usually, but not necessarily, selected as the mixture fraction. This can be seen when the conservation equations for the species and energy are transformed using a conserved scalar as an independent coordinate, i.e., $\varphi = \varphi(t, x_1, x_2, x_3) = \varphi(\tau, f, x_2, x_3)$ where $t = \tau$ and $f = f(t, x_1, x_2, x_3)$. This transform can be made, by selecting an original coordinate system such that x_1 does not lie in the flame surface and consequently a single-valued function $x_1 = x_1(t, f, x_2, x_3)$ can be obtained. Assuming unity of Lewis numbers and considering that the reaction occurs in a thin layer, the flamelet equations to leading order can be written as [7, 16, 18, 19]

$$\rho \frac{\partial Y_i}{\partial \tau} - \frac{\rho \chi}{2} \frac{\partial^2 Y_i}{\partial f^2} = \dot{m}_i \tag{13}$$

$$\rho c_p \frac{\partial T}{\partial \tau} - \frac{\rho c_p \chi}{2} \frac{\partial^2 T}{\partial f^2} = -\sum_{i=1}^{n} h_{i0} \dot{m}_i + q_r + \frac{\partial p}{\partial t} \tag{14}$$

where χ is the scalar dissipation rate $2D\nabla f \bullet \nabla f$ which can be considered as the inverse of the diffusion time scale. The counter flow diffusion flame was proposed in [16] as the representative laminar flamelet. This representative provides a relation between scalar dissipation and mixture fraction as $\chi = \chi_{st} \frac{f^2}{f_{st}^2} \frac{\ln f}{\ln f_{st}}$, where the subscript st denotes stoichiometry.

If we ignore the time related derivative (the first term on the l.h.s) of Eq. 14, the flamelet structure is described by a set of one-dimensional second order differential equations, with χ_{st}, q_r and p acting

as parameters. If we further assume small variations of q_r and p, the solution is then determined by the scalar dissipation rate χ_{st} and the flamelet equations' boundary conditions in the conserved scalar space. Two independent boundary conditions are normally necessary and sufficient for each dependent variable. The flamelet equations can be derived locally, but in the same form, on the flame surface. In order to have a universal solution characterized by the single conserved scalar, which essentially provides the ease and possibility of applying the flamelet model in turbulent combustion modeling, the boundary conditions of the flamelet equations should also be location independent. A typical configuration, which meets this requirement, is the two-feed system. For a proper set of boundary conditions, the steady flamelet structure is given by $Y_i = Y_i(f, \chi_{st})$, $T = T(f, \chi_{st})$. This flamelet structure can be obtained from detailed experimental measurements [34-36] or theoretical laminar flame calculations [37, 38]. As mentioned above, the conserved scalar f does not necessarily need to be the conventional mixture fraction. It can be considered as a general variable, which fulfills the conservation $\frac{\partial(\rho f)}{\partial t} + \frac{\partial(\rho u_i f)}{\partial x_i} = \frac{\partial}{\partial x_i}(\rho D \frac{\partial f}{\partial x_i})$ and allows the reduction of the flamelet equations to the leading order form so that the flamelet structure can be described using this conserved scalar as the coordinate. The assumption of unity Liews numbers brings the simplicity to the flamelet equations. This assumption can be lifted to consider the differential diffusion [39] when the effect of non-equal Liews numbers is important.

The above discussion gives an important hint that in the turbulent non-premixed combustion modeling, if we assume the turbulent flame is an ensemble of laminar flamelets of well defined structure, the detailed chemistry computation could be separated from the flow field calculation, and the modeling can be proceeded by finding out the flamelet statistics, which can be represented by a probability density function (pdf) $\widetilde{p}(f, \chi_{st})$. The mean mass fraction in a turbulent flame is evaluated from the laminar flamelet structure and the statistics of the related conserved scalar and the scalar dissipation rate as

$$\widetilde{Y}_i = \int_0^\infty \int_0^1 Y_i(f, \chi_{st}) \widetilde{p}(f, \chi_{st}) df \, d\chi_{st} \tag{15}$$

If f and χ_{st} are assumed statistically independent, then the above equation becomes

$$\widetilde{Y}_i = \int_0^\infty \left[\int_0^1 Y_i(f, \chi_{st}) \widetilde{p}(f) df \right] \widetilde{p}(\chi_{st}) d\chi_{st} \tag{16}$$

In a turbulent reacting flow, the local pdf is very difficult to obtain, but can be approximately prescribed or estimated from the solution of a carefully constructed pdf transport equation [40-43]. The prescribed pdf, $\widetilde{p}(f)$, can be constructed from the mean mixture fraction and its variance, for example, using the normalized Beta [15, 17, 20], clipped Gaussian function [44] or top hat functions [45]. In this thesis, a prescribed normalized Beta function pdf is used. The normalized Beta function has only two parameters and can approximate reasonably well the usual pdf shape found in a jet when the parameters are properly given. In some situations, the simulation of a turbulent reacting flow may not be sensitivity to the specific pdf shape [45].

The pdf constructed using the normalized Beta function can be written as

$$p(f) = \frac{f^{\alpha-1}(1-f)^{\beta-1}}{\int_0^1 f^{\alpha-1}(1-f)^{\beta-1}\,df} \tag{17}$$

where the function parameters α and β can be related to the mean mixture fraction and variance as $\alpha = \tilde{f}\left[\tilde{f}(1-\tilde{f})/\tilde{g} - 1\right]$, $\beta = \alpha(1-\tilde{f})/\tilde{f}$.

The third hypothesis of Kolmogorov states that the logarithm of the dissipation rate, averaged in a space much smaller than the integral scale, has a normal distribution [8]. Assuming a log-normal distribution of χ, the prescribed $\tilde{p}(\chi)$ can be constructed as [15, 17]

$$\tilde{p}(\chi) = \frac{1}{\chi\sigma\sqrt{2\pi}}\exp\left\{-\frac{1}{2\sigma^2}(\ln\chi - \mu)^2\right\} \tag{18}$$

where the parameters μ and σ are related to the mean and variance of χ as

$$\tilde{\chi} = \exp(\mu + 0.5\sigma^2) \tag{19}$$

in which σ can be estimated from $\sigma^2 = 0.5\ln(0.1\mathrm{Re}^{0.5})$, and $\tilde{\chi}$ can be modeled by

$$\tilde{\chi} = c_{g2}\frac{\tilde{g}\varepsilon}{k} \tag{20}$$

Both mean mixture fraction and its variance are given by the solution of their transport equations

$$\frac{\partial(\bar{\rho}\tilde{f})}{\partial t} + \frac{\partial(\bar{\rho}\tilde{u}_j\tilde{f})}{\partial x_j} = \frac{\partial}{\partial x_j}\left(\frac{\mu}{S_c}\frac{\partial\tilde{f}}{\partial x_j} - \bar{\rho}\overline{u_j''f''}\right) \tag{21}$$

$$\frac{\partial(\bar{\rho}\tilde{g})}{\partial t} + \frac{\partial(\bar{\rho}\tilde{u}_j\tilde{g})}{\partial x_j} = \frac{\partial}{\partial x_j}\left(\frac{\mu}{S_c}\frac{\partial\tilde{g}}{\partial x_j} - \bar{\rho}\overline{u_j''g}\right) - 2\bar{\rho}\overline{u_j''f''}\frac{\partial\tilde{f}}{\partial x_j} - c_g\bar{\rho}\tilde{g}\frac{\varepsilon}{k} \tag{22}$$

where $\tilde{g}$ is the variance of the mixture fraction $\tilde{f}''^2$.

The second moments in the above two equations can be modeled as discussed in the turbulence model section.

When using the flamelet steady state library $Y_i(f, \chi_{st})$, it is implied that the flamelet in a turbulent reacting system can adjust itself quickly to the local condition, so that the flamelet can reach the steady state. However, this may not always be valid. In the fast processes, such as those in internal

combustion engines, the flamelet may not be able to adjust itself instantaneously to its local flow condition. In this case, the evolution history of the flamelet may have important effect. Therefore, the flamelet's evolution under transient local flow condition should be followed. In this case, the time derivative term in the flamelet equation cannot be dropped and the flamelet equation should be solved interactively with the flow solution, which provides the flamelet parameters such as χ_{st} and p, but the chemistry computation can still be separated from flow calculation. This concept is the so-called Representative Interactive Flamelet (RIF) [46-48] method.

Because the temperature is strongly dependent on the radiation, the assumption that it is a function of mixture fraction alone is unjustified. To account for radiation, the energy equation can be solved and the mean temperature evaluated from the mean enthalpy using an approximate Favre average of Eq. 5: $\widetilde{h} = \sum \widetilde{Y}_i \left(h_{0,i} + \int_{T_0}^{\widetilde{T}} c_{p,i} d\widetilde{T} \right)$.

In this model, the transport equation for mean mass fraction is not solved and thus the mean reaction rate does not need to be directly modeled.

3.1.5 Soot modeling

Soot is of great interest for various reasons. The soot emitted from combustion poses a pollution threat to the environment. It can enhance the desired radiation heat transfer in industrial furnaces and the undesired radiation heat transfer in fires. Soot is also used in many fire detection systems.

Soot is a product of incomplete combustion of hydrocarbon fuels. In premixed flames, the hydrocarbon fuel will break into small hydrocarbon radicals when passing through the high temperature zone. From these radicals, small hydrocarbon molecules like acetylene can be formed. Under fuel rich conditions, the small molecules and radicals can react to form aromatic rings. Through 'planar growth' and coagulation, small soot particle nuclei can be formed from PAH. This process is the particle inception. The formed small particle will quickly coagulate and pick up gas phase component for surface growth. The coagulation determines the final soot particle size, while the surface growth is critical for the final soot volume fraction. The surface growth is mainly through the HACA (H Abstraction Carbon Addition) mechanism and its rate is largely dependent on the number of active sites on the soot particle surface. The activity of soot particle surface can decrease quickly with residence time. The formed soot might be oxidized by O_2 and OH when transported to the lean region. The oxidation may be frozen when the temperature drops below about 1300 K [49], and then the unoxidized soot will be emitted. In diffusion flames, soot formation process is similar from the first ring. It is largely the initial stage that makes difference. In diffusion flames, since soot is formed in fuel rich and relatively low temperature zone, the molecular structure of the parent fuel has more importance for soot tendency than in premixed flames [49, 50].

Modeling of soot formation and oxidation is a prohibitive task. In this thesis, only the modeling of soot in diffusion flames is of interest and will be briefly discussed below.

Since surface growth and oxidation are heterogeneous slow processes, there is no strict state relation between the soot volume fraction and the mixture fraction and the classical flamelet concept is thus

not applicable. However, it may be argued that the soot formation and oxidation rates can be approximated as a function of mixture fraction. Therefore, with the reaction source term provided, soot can be modeled within the framework of flamelet concept by solving additional transport equations.

In recent years, significant progress has been made in soot modeling [51]. Moss has presented a two-variable soot model [52-55] which includes the essential physics. With the model parameters carefully adjusted through calibration, his model has been shown to be quite successful. A similar two-variable soot model was proposed by Lindstedt [56, 57] and was quite successfully applied to turbulent soot modeling [58, 59]. In this soot model, soot formation is related to the chemical intermediate acetylene, rather than to the parent fuel, which was used in the soot model suggested by Moss et al [52-55]. Recently, Mauss et al. [60] have presented a soot model in which the transport equation for soot volume fraction was solved with the source terms calculated in the mixture fraction/scalar dissipation rate space for laminar flamelets and tabulated in a library. In these models, based on the flamelet concept, the reaction rates of soot formation and oxidation are eventually considered as a function of mixture fraction alone.

The soot model proposed by Lindstedt was incorporated and coupled with other model in a study of flame heat transfer [cf. paper 4]. The Mauss's soot model was adopted and coupled into CFD to study the sooting in a C3H6 buoyant diffusion flame. This computation will be validated against experimental data and the detail will be reported in a future publication. The preliminary result is shown in Fig. 3.

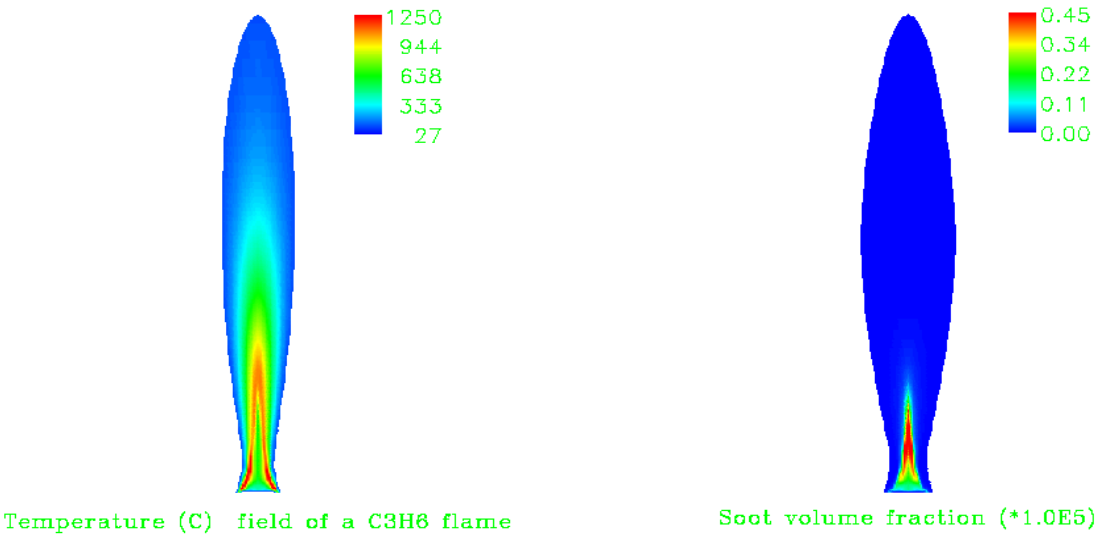

Fig. 3 Temperature and soot volume fraction distribution in a C3H6 flame

The application of the above-mentioned types of soot model is still limited to simple fuels. For complex fuels, as an estimation, simple empirical models based on measurement data can be used [cf. papers 1 and 3].

3.1.6 Radiation modeling

Due to its strong dependence on temperature and the strong radiating behavior of combustion products, thermal radiation is an important heat transfer mechanism in many combustion systems.

Thermal radiation can be defined as electromagnetic waves emitted by a medium solely due to its temperature. The wavelength range important to heat transfer is normally limited between $0.1\mu m$ (ultraviolet) and $100\,\mu m$ (midinfrared).

3.1.6.1 Radiation transfer equation (RTE) and its solution

For a medium in local thermodynamic equilibrium, the differential equation of the spectral radiation can be written as [61, 62]

$$\frac{\partial I_{w,s}}{\partial s} = k_{w,s} I^0_{w,s} - \beta_{w,s} I_{w,s} + \frac{\sigma_{w,s}}{4\pi} \int_{4\pi} I_{w,s}(\vec{s}_i)\Phi(\vec{s}_i, \vec{s})d\Omega_i \tag{23}$$

where the superscript 0 stands for black body radiation, $k_{w,s}$ is the effective spectral absorption coefficient which includes effects of both induced absorption and induced emission, $\sigma_{w,s}$ the spectral scattering coefficient, $\beta_{w,s}$ the extinction coefficient $\beta_{w,s} = k_{w,s} + \sigma_{w,s}$, $\vec{s}_i$ and $\vec{s}$ the direction vectors, and $\Phi(\vec{s}_i, \vec{s})$ the phase function, which is equal to 1.0 for isotropic scattering. The three terms on the right side represent the augmentation due to emission, the attenuation due to absorption and scattering, and the augmentation due to scattering, respectively. Since the light speed in a medium is usually large, the radiation time scale is much smaller than almost all the other practical time scales concerned in combustion engineering, the transient term has been ignored in the above equation.

The spectral radiation transfer equation is usually rewritten using non-dimensional optical coordinate as

$$\frac{\partial I_{w,s}}{\partial x_w} + I_{w,s} = (1.0 - \omega_w) I^0_{w,s} + \frac{\omega_w}{4\pi} \int_{4\pi} I_{w,s}(\vec{s}_i)\Phi(\vec{s}_i, \vec{s})d\Omega_i = S_w(x_w, \vec{s}) \tag{24}$$

where the single scattering albedo ω_w is defined as $\omega_w = \frac{\sigma_{w,s}}{\beta_{w,s}}$, $x_w = \int_0^s \beta_{w,s} ds$ and the source function $S_w(x_w, \vec{s}) = (1.0 - \omega_w) I^0_{w,s} + \frac{\omega_w}{4\pi} \int_{4\pi} I_{w,s}(\vec{s}_i)\Phi(\vec{s}_i, \vec{s})d\Omega_i$.

The rewritten RTE is an integral-differential equation. Multiplying this RTE by e^{x_w} results in

$$\frac{\partial (I_{w,s} e^{x_w})}{\partial x_w} = S_w(x_w, \vec{s}) e^{x_w} \tag{25}$$

which can be integrated along the radiation path from an arbitrary point s_1 to another arbitrary point s_2 to give

$$I_{w,s_2} e^{x_{w,s_2}} = \int_{x_{w,s_1}}^{x_{w,s_2}} S_w(x_w, \vec{s}) e^{x_w} dx_w + I_{w,s_1} e^{x_{w,s_1}} \tag{26}$$

This integration can be rewritten as

$$I_{w,s_2} = \int_{x_{w,s_1}}^{x_{w,s_2}} S_w(x_w, \vec{s}) e^{-(x_{w,s_2} - x_w)} dx_w + I_{w,s_1} e^{(x_{w,s_1} - x_{w,s_2})}$$

$$= \int_{x_{w,s_1}}^{x_{w,s_2}} S_w(x_w, \vec{s}) d(e^{-(x_{w,s_2} - x_w)}) + I_{w,s_1} e^{(x_{w,s_1} - x_{w,s_2})} \tag{27}$$

where $e^{-(x_{w,s_2} - x_w)}$ is the transimissivity from point s to point s_2.

The above solution is a third order integral equation, where the source function itself is an integration of unknown radiation intensity.

The radiation path is usually non-gray and non-homogeneous. Due to its complexity, an exact solution can only be obtained for a few simple cases. For most practical applications, solutions are obtained using engineering approximation methods.

Once the radiation intensity field is solved (or assumed known), the spectral heat flux vector and radiation energy source term can be readily calculated as

$$\vec{q}_w = \int_{4\pi} I_w(\vec{s}) \vec{s} \, d\Omega \tag{28}$$

$$\nabla \bullet \vec{q}_w = \nabla \bullet \int_{4\pi} I_w(\vec{s}) \vec{s} \, d\Omega = \int_{4\pi} \vec{s} \bullet \nabla I_w(\vec{s}) d\Omega = \int_{4\pi} \frac{\partial I_w(\vec{s})}{\partial s} d\Omega$$

$$= \int_{4\pi} (k_{w,s} I_{w,s}^0 - \beta_{w,s} I_{w,s} + \frac{\sigma_{w,s}}{4\pi} \int_{4\pi} I_{w,s}(\vec{s}_i) \Phi(\vec{s}_i, \vec{s}) d\Omega_i) d\Omega$$

$$= k_{w,s} (4\pi I_w^0 - \int_{4\pi} I_w(\vec{s}) d\Omega) \tag{29}$$

During the derivation of Eq. 29, the integration order has been changed and use has been made of the fact that $\nabla \bullet (a\vec{b}) = \nabla a \bullet \vec{b} + a \nabla \bullet \vec{b}$ and that the space and direction coordinates are independent.

3.1.6.2 Boundary conditions for RTE

Since radiation is generally a long-range phenomenon and the RTE is a differential equation, the radiation transfer equation should be solved in a bounded volume with the proper boundary conditions provided at all the volume surfaces.

For a general opaque surface, the boundary condition can be written as

$$I_w(\vec{r},\vec{s}) = \in_w (\vec{r},\vec{s}) I_w^0(\vec{r}) + \int_{\vec{n}\bullet\vec{s}'<0} \rho''_w(\vec{r},\vec{s},\vec{s}') I_w(\vec{r},\vec{s}') \left|\vec{n}\bullet\vec{s}'\right| d\Omega' \tag{30}$$

where $\in_w (\vec{r},\vec{s})$ is the spectral directional emissivity and $\rho''_w(\vec{r},\vec{s},\vec{s}')$ the spectral bidirectional reflection function.

When the surface emits and reflects diffusely, this condition is reduced to

$$I_w(\vec{r}) = \in_w (\vec{r}) I_w^0(\vec{r}) + \frac{1}{\pi}(1-\in_w (\vec{r})) \int_{\vec{n}\bullet\vec{s}'<0} I_w(\vec{r},\vec{s}') \left|\vec{n}\bullet\vec{s}'\right| d\Omega' \tag{31}$$

The above boundary conditions should be modified to include the transimission when the boundary is transparent or semi-transparent. In this case, the emissivity can be considered as an effective property of in-depth medium. An opening to the environment can be approximated as a cold black body.

3.1.6.3 Discrete transfer (DT) method

There are a number of approximate methods to solve the RTE and obtain $\overline{S}_h$ and radiation heat flux to surfaces, including the spherical harmonics method (P_N approximation), discrete ordinates method (S_N approximation), discrete transfer method, zonal method and Monte Carlo method. In this thesis, the discrete transfer method [63] is employed and will be briefly presented below. The discussion of other methods can be found in [62].

DT is one of the most popular methods used in the numerical calculation of radiation. It combines some features of the discrete ordinates, zonal and Monte Carlo methods and has the advantages of good accuracy, economy and flexibility for complex geometries.

This method solves the radiation equation along a discrete set of directions (rays) from every element of the boundary surface. Taking the surface element P_j shown in Fig. 4 as an example, with the boundary condition and the participating medium properties provided, RTE is solved along the every representative irradiation ray, such as the ray $Q_i \to P_j$, to give the radiation intensity along every irradiation ray. The incident radiation flux at surface element P_j can then be calculated as

$$H_{w,p_j} = \vec{q}_{w,p_j} \bullet \vec{n} = \int_{\vec{s}\bullet\vec{n}<0} I_w(P_j,\vec{s})\vec{s}\bullet\vec{n}\,d\Omega \approx \sum_{i=1}^{N\,rays} I_w(P_j,\vec{s}) \cos\theta_{j,i} \Delta\Omega_{j,i}$$

$$\approx \sum_{i=1}^{N\,rays} I_w(P_j,\vec{s})\cos\theta_{j,i}\sin\theta_{j,i}\sin(\Delta\theta_{j,i})\Delta\varphi_{j,i} \tag{32}$$

where $\theta_{j,i}$ is the angle between the surface normal vector and the incident ray direction.

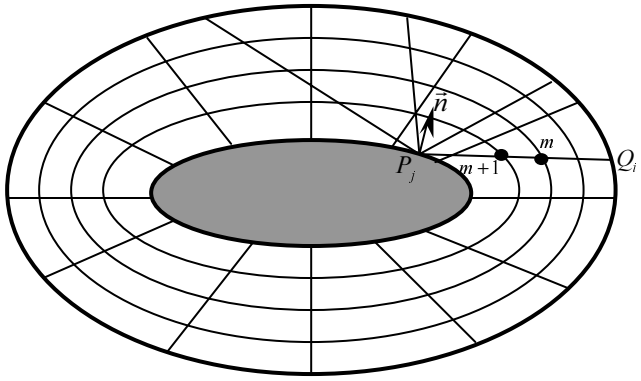

Fig. 4 Illustration of discrete transfer method

The radiation source from a specific irradiation ray $Q_i \to P_j$ for a general control volume m is evaluated as

$$S_{w,m,Q_i\to P_j} = (I_{w,m+1,Q_i\to P_j} - I_{w,m,Q_i\to P_j})A_{P_j}\cos\theta_{j,i}\Delta\Omega_{j,i} \tag{33}$$

where the assumption is made that the radiation intensity inside the beam of the ray is uniform and the ray crossing the control volume is completely overlapped by the control volume.

The sum of $S_{w,m,Q_i\to P_j}$ over all possible crossing rays approximately gives the spectral radiation source for the control volume m. The total radiation source, which provides the energy source for the enthalpy transport equation, is then obtained simply by numerical quadrature of the spectral radiation source over the whole spectrum.

3.1.6.4 Model test against exact solutions

Exact solutions for simple cases are normally used for model testing and code verification. Heaslet and Warming [64] presented the exact solution for radiative equilibrium one dimensional medium between two parallel black isothermal plates. The participating medium is isotropic and gray with a constant absorption coefficient. Fig. 5 and Table 1 compare the numerical and exact solutions and show good agreement.

Dua and Cheng [65] gave an exact solution for radiation in a finite cylinder, which has a radius of reference L and a height of 2L. The medium inside the cylinder has constant and uniform absorption coefficient and temperature T_g. The comparison of numerical calculations with exact solutions is shown in Fig.6 for different optical thickness. A good agreement can be seen.

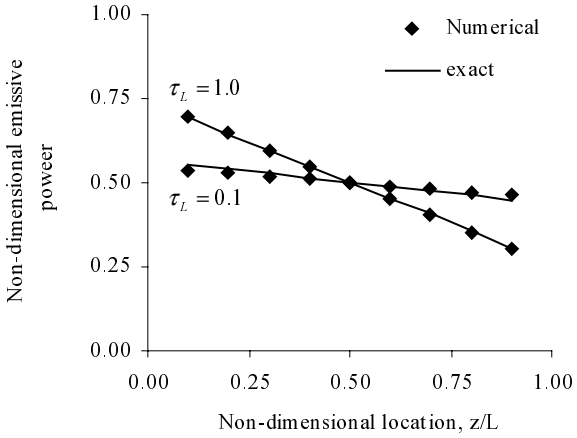

Fig. 5 Non-dimensional temperature distribution for radiative equilibrium between parallel plates. Note: z is the distance from a plate surface, the non-dimensional emissive power is defined as $\frac{T^4 - T_2^4}{T_1^4 - T_2^4}$ and τ_L is the optical thickness kL, where k is the absorption coefficient and L is the distance between plates.

τ_L	Ψ_b (exact)	Ψ_b (numerical)	τ_L	Ψ_b (exact)	Ψ_b (numerical)
0.1	0.9157	0.9162	1.5	0.4572	0.4484
0.3	0.7934	0.7894	2.0	0.3900	0.3826
0.5	0.7040	0.6966	2.5	0.3401	0.3341
0.6	0.6672	0.6588	3.0	0.3016	0.2967
1.0	0.5532	0.5437	5.0	0.2077	0.2062

Table 1 Non-dimensional radiative heat flux for radiative equilibrium between parallel plates. Note: Ψ_b is the non-dimensional radiative flux $\Psi_b = \frac{q_r}{\sigma(T_1^4 - T_2^4)}$, where T_1 and T_1 are the temperatures of the parallel plates.

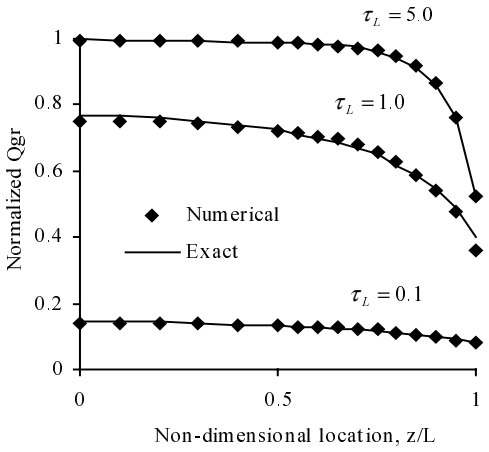

Fig. 6 Non-dimensional gas radiative flux along z direction on the cylinder wall. Note: $Q_{gr} = q/\sigma T_g^4$, z=0 at the middle height of the cylinder.

It is worthy to mention that DT is an approximation method. The necessary ray number is dependent on the case geometry and the spatial uniformity of the radiating medium.

3.1.6.5 Radiation property evaluation

The radiation property of the radiating medium must be evaluated when solving the radiation equation. Commonly adopted radiation property evaluation methods are total absorbtivity method [66], weighted sum of gray gas (WSGG) method [66], wide band model [67] and narrow band model [68].

In combustion system, radiation comes from both gases and particles. The radiating gases normally include water vapor, carbon dioxide, hydrocarbon fuels and carbon monoxide, etc. The particles include mainly soot and possibly other particles such as pulverized coal and ash.

Radiating gas and soot have quite different radiation behavior. At the moderate temperature, in the gas, the energy level transitions mainly happen as bound-bound transition, and bound-free and free-free transitions are rare. According to quantum theory, the molecule energy levels are quantitized. As a result, the radiating gases are highly non-gray showing strong band radiation. Water vapor and carbon dioxide are usually the main radiating gases in a combustion system, having their most important infrared radiation bands centred at 1.38, 1.87, 2.7 and 6.3 microns for water vapor, 2.7 and 4.3 microns for carbon dioxide. The diatomic molecules including oxygen and nitrogen do not radiate at normal combustion temperature. In some situations, the gas fuels and their intermediates may play an important role in radiation. According to Mie's scattering theory, the scattering efficiency factor is proportional to the fourth power of the particle's size parameter. Since the gas molecules are much smaller than the thermal radiation wavelength, their contribution to the scattering is negligible.

Soot particle radiation includes both scattering and absorption/emission, but the scattering can also be ignored when the particle is sufficiently small. Soot shows a spectrally continuous radiation and is quite gray since its spectral absorption coefficient is a weak function of the wavelength (approximately proportional to the inverse of wavelength when the particles are small).

(1) Spectral radiation of gases

The spectrum of a radiating gas consists of a large number of individual radiation lines. Each individual line corresponds to a transition between two molecular quantitized energy levels. However, the individual line is not exactly monochromatic. It is broadened by nature broadening, collision broadening and Doppler broadening. Thus, each individual line has some finite width. The shape of collision broadened line is the same as that of nature broadened line, but differs from that of Doppler broadened line. The width of the broadened line is dependent on the broadening mechanism and the mixture's thermal state. Since collision broadening results from molecule's collisions which are proportional to molecule's number density and average speed, it is not surprising that the half width of the collision line is proportional to $\frac{p}{\sqrt{T}}$. The Doppler line's half width is, on the contrary, proportional to $\sqrt{T}$ and the wave number. When calculating radiation, all the broadening mechanisms should be considered in principle. But usually the collision broadening is much more important and the problem can be simplified. When the collision line's half width is 2 or 3 times more than that of the Doppler line, the Doppler broadening can be ignored. At high temperature and/or low pressure, due to the different variation behaviors of the half widths of collision and Doppler lines, and that the shift of the important part of Planck function to large wavenumber spectrum, the Doppler line can become important.

(2) Spectral radiation of soot particle

The radiation behavior of soot particle varies with the detail chemical composition of the particle. This variation can be very complex, and is thus often ignored. Assuming the soot particles are sufficiently small that the scattering can be ignored, we have [62]

$$Q_{abs} \approx -4\Im\left(\frac{m^2-1}{m^2+2}\right)\bullet\frac{2\pi r}{\lambda} \tag{34}$$

$$k_\lambda = \int_0^\infty \pi r^2 n_p(r) Q_{abs} dr = -6\Im\left(\frac{m^2-1}{m^2+2}\right)\frac{\pi}{\lambda}\int_0^\infty \frac{4}{3}\pi r^3 n_p(r) dr \tag{35}$$

where Q_{abs} is the absorption efficiency factor, r the radius of the idealized spherical particle, $n_p(r)$ particle number density, $\Im$ denotes the image part and $\int_0^\infty \frac{4}{3}\pi r^3 n_p(r) dr$ gives the soot volume fraction f_v.

The above equation can further be written as

$$k_\lambda = -\Im\left(\frac{m^2-1}{m^2+2}\right)\frac{6\pi f_v}{\lambda} = \left(\frac{36\pi nk}{(n^2-k^2+2)^2+4n^2k^2}\right)\frac{f_v}{\lambda} \tag{36}$$

which indicates that the spectral radiation absorption coefficient of a soot cloud of small particles is proportional to the soot volume fraction and inversely proportional to the wave length.

The complex refractive index is dependent on the particle's chemical composition, which is expected to vary with fuel type. Hottel and Sarofim [66] suggested a value of about 7.0 for $\frac{36\pi nk}{(n^2-k^2+2)^2+4n^2k^2}$. Therefore, we approximately have $k_\lambda \approx 7.0\frac{f_v}{\lambda}$.

When computing particle radiation, it is usually assumed that the soot particle has the same temperature as the immediate surrounding gas. The validity of this assumption can be supported by the small particle size assumption. For a spherical particle of diameter D in the gas, the convection heat transfer N_u number can be written as [69]

$$\overline{N}_{uD} = \frac{h_c D}{\lambda} = 2.0 + 0.6 R_{eD}^{1/2} P_r^{1/3} \tag{37}$$

where h_c is the convection heat transfer coefficient, λ the thermal conductivity of the gas. The above equation indicates that the smaller the particle size, the higher the convection heat transfer coefficient, the quicker the particle follows the gas temperature history. This is the same as that which explains why a small thermal couple is preferred in order to minimize the uncertainty of gas temperature measurement in a combustion system.

(3) Narrow band model for a constant parameter path

The spectrum of a radiating gas is usually highly complex. Although the exact solution of gas radiation can be obtained in principle by line-by-line calculation, it requires huge computation effort and all the detailed information of the individual lines, and is thus prohibitive. This necessitates the approximation method of introducing models. The narrow band model is the most accurate engineering method for the evaluation of radiation properties. In the narrow band model, the evaluation is carried out, not on every individual line, but on small spectrum intervals, which are normally at $5-50\ cm^{-1}$. Within each narrow band, there are many individual lines. Therefore, the purpose of narrow band models is to approximate the mean radiation properties within the small spectrum intervals. In order to extract their mean radiation properties, the information about the strength distribution, spacing, width and shape of the individual lines are needed. This information usually turns out to be very complicate. As a result, approximations are introduced when constructing the narrow band models. The line broadening mechanism describes the line shape and its width. Most important assumptions are related to line strength distribution and line spacing. Different approximations on line distribution and line spacing result in different narrow band models. The choice of a specific narrow band model can be based on accuracy and mathematical simplicity. The accuracy of a particular narrow band model relies on how well its assumptions comply with the

spectrum structure of the radiating molecule being considered. The regular model (Elasser model) is more appropriate for the simple molecules which have approximately equal line space and line strength, particularly when the Q branch is not important or even presented. For complex molecules which have irregular line strength distribution and line spacing, the random (statistical) model can be more applicable.

The spectral absorption coefficient at any wavenumber can be calculated as a sum of the contribution from all the individual lines

$$k_w = \sum_i k_{wi} \tag{38}$$

The mean spectral (narrow band) absorption coefficient and emissivity can be calculated from

$$\bar{k}_w = \frac{1}{\Delta w}\int_{w-\frac{\Delta w}{2}}^{w+\frac{\Delta w}{2}} k_{w'}\,dw' \tag{39}$$

$$\bar{\varepsilon}_w = \frac{1}{\Delta w}\int_{w-\frac{\Delta w}{2}}^{w+\frac{\Delta w}{2}} \left[1-\exp(-\int_0^s k_{w'}\,ds)\right]dw' \tag{40}$$

Since ε is a non-linear function of k, $\bar{\varepsilon}_w$ cannot be simply written as $\varepsilon_w(\bar{k}_w)$, even for a homogeneous and isothermal path. This point is important and similar to that in turbulent combustion modeling where the mean reaction rates cannot be given solely by the mean temperature and mean concentrations.

Narrow band model gives the approximations for $\bar{k}_w$ and $\bar{\varepsilon}_w$. In this thesis, the so-called Goody model is adopted for the collision line and a random model of equal line strength is adopted for Doppler line. They will briefly be presented below.

Goody model is a random model for the collision line, where an exponential line strength distribution is assumed, i.e., $P(S) = \frac{4}{\pi S_E}\exp(-\frac{4S}{\pi S_E})$. The optical thickness for a constant parameter path is approximately given by [68]

$$X_c = X^*(1+X^*/4a_c)^{-1/2} \tag{41}$$

where X^* is the optical depth in the weak line limit, presented by

$$X^* = \bar{k}_w u \tag{42}$$

and a_c is the collision broadened fine structure parameter defined as

$$a_c = \frac{\gamma_c}{d} \tag{43}$$

In the above equations, u is the optical path length, γ_c the half width of the collision line, d the line spacing and $\bar{k}_w$ the mean absorption coefficient in the weak line limit, which is equal to the mean line-strength-to-spacing parameter $\overline{S/d}$. $\overline{S/d}$ and $1/d$ are the two important band parameters. Both are functions of temperature and wavenumber. It is important to note that both u and $\bar{k}_w$ are reduced here to the reference state of standard temperature and pressure.

According to the random model of equal line strength, i.e. $P(S) = \delta(S - S_0)$, the optical path thickness of a Doppler line is given by

$$X_D = 1.7 a_D \left\{ \ln\left[1 + \left(0.589 X^* / a_D \right)^2 \right] \right\}^{0.5} \tag{44}$$

where a_D is the Doppler broadened fine structure parameter

$$a_D = \frac{\gamma_D}{d} \tag{45}$$

with γ_D defined as the half line width of the Doppler line.

A function is used to combine collision and Doppler broadened optical depths to give the overall optical depth

$$X = -\ln \tau = X^* (1 - y^{-0.5})^{0.5} \tag{46}$$

in which y is given by

$$y = \left[1 - \left(\frac{X}{X^*} \right)^2 \right]^{-2} + \left[1 - \left(\frac{X_D}{X^*} \right)^2 \right]^{-2} - 1 \tag{47}$$

(4) The Curtis-Godson approximation

The Curtis-Godson approximation provides a two parameter representation of the optical depth for a general non-homogeneous non-isothermal path. These two parameters and the approximation function are identified by certain imposed conditions. The approximation should give the known exact solutions at some limit regimes and return to the exact formula for a constant parameter path. For a collision line, the optical depth of a general path is $X_c = \int_0^u \bar{k}_w du'$ at the weak line limit and

$X_c = 2(\int_0^u \bar{k}_w \frac{\gamma_c}{d} du')^{0.5}$ at the strong line limit. The optical depth of the collision line for a constant parameter path is given before as $X_c = \bar{k}_w u(1+\bar{k}_w u/4a_c)^{-1/2}$. These conditions define the optical depth of the collision line for a general path as

$$X_c = X^*(1+X^*/4a_c)^{-1/2} \tag{48}$$

where X^* and a_c are now given by

$$X^* = \int_0^u \bar{k} du' \tag{49}$$

$$a_c = \frac{1}{X^*}\int_0^u \bar{k}\frac{\gamma_c}{d} du' \tag{50}$$

Similarly, for a Doppler line, we have

$$X_D = 1.7a_D\left\{\ln\left[1+\left(0.589X^*/a_D\right)^2\right]\right\}^{0.5} \tag{51}$$

where a_D is given by

$$a_D = \frac{1}{X^*}\int_0^u \bar{k}\frac{\gamma_D}{d} du' \tag{52}$$

The Curtis-Godson approximation has only two parameters. The limiting conditions imposed on the development of the Curtis-Godson approximation may not be sufficient to guarantee the accuracy, particularly when the temperature variation along the path is sharp. In order to reduce the error, which may be introduced by the Curtis-Godson approximation, the radiating lines can be divided into multiple groups. Within each group, the lines have similar temperature dependence. This results in the Multiple Line Group (MLG) model [68].

(5) Narrow band computation of the radiation of hydrocarbon gas fuels

The radiation of hydrocarbon gas fuels is of interest since it may significantly affect the ignition and combustion of the condensed fuels. The hydrocarbon gas fuel arising from the evaporation and decomposition of the condensed fuel may form a surrounding fuel vapor layer. This gas fuel layer can build up the radiation blockage and thus attenuate the radiant feedback from the flame to the condensed fuel surface [70, 71].

Brosmer and Tien made low resolution spectral radiation measurements for some hydrocarbon gas fuels including C3H6 and C2H2 [72, 73]. The spectral data of C3H6 and C2H2 have been incorporated into narrow band computation in a cooperative research on radiation blockage with J. deRis (FMRC, USA).

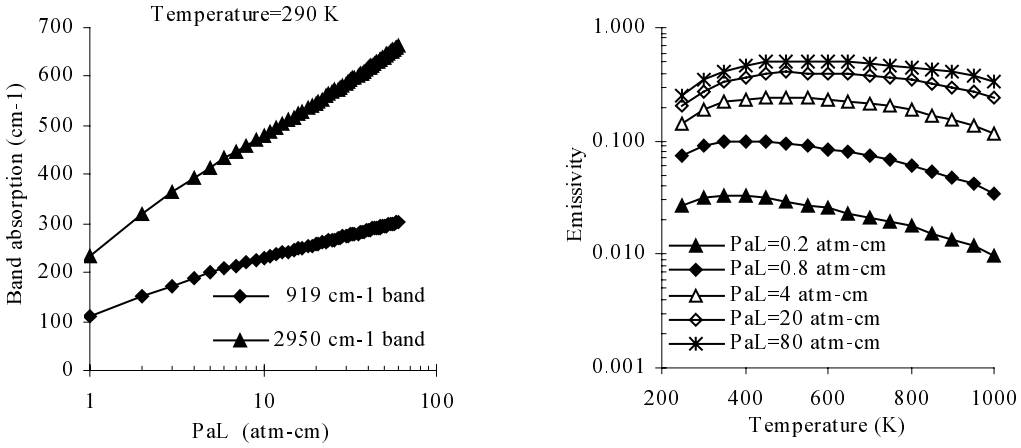

Fig. 7 Band absorption and emissivity of C3H6. Note: PaL is the pressure path length.

The main C3H6 infrared radiation bands are centered at 3.4, 5.5, 6.1, 6.9 and 10.8 microns. The narrow band calculations of its band absorption and emissivity are shown in Fig. 7, which are in good agreement with Brosmer and Tien's measurements and the wide band model correlation [cf. Ref. 72].

The important C2H2 infrared radiation bands are at 3.04, 7.53 and 13.7 microns. Fig. 8 shows the narrow band calculations of its band absorption and emissivity, which agree well with Brosmer and Tien's measurements and the wide band model correlation [cf. Ref. 73], while the difference starts to appear in the emissivity data at high pressure path lengths.

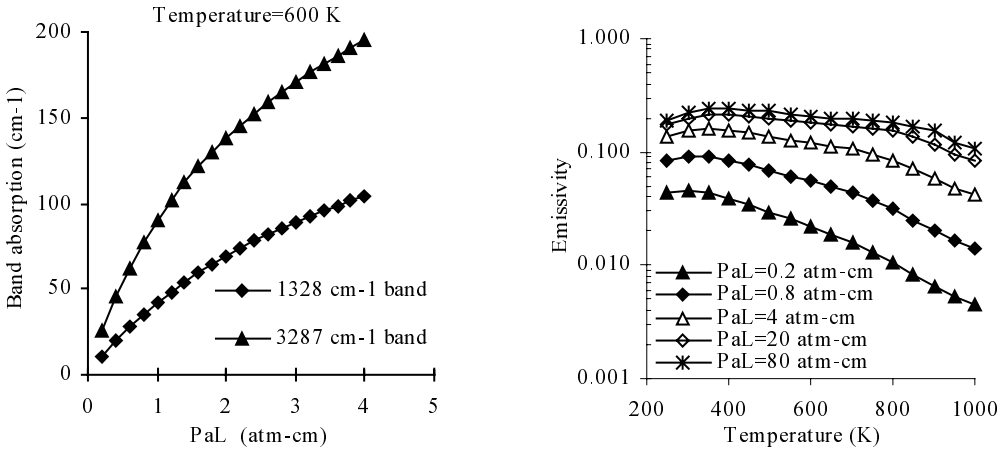

Fig. 8 Band absorption and emissivity of C2H2

(6) Development of a fast narrow band model (FASTNB)

The narrow band model is the most accurate engineering approximation method, but it is usually expensive to implement. The speed of narrow band computation is of critical importance. In this thesis, a fast narrow band computer model, FASTNB, which predicts the radiation intensity in a generally non-isothermal and non-homogeneous combustion environment was developed. FASTNB provides an accurate calculation at reasonably fast speed. When compared with Grosshandler's narrow band model, RADCAL [74], which has been verified quite extensively against experimental measurements, FASTNB is more than 20 times faster and gives almost exactly the same result as RADCAL, as shown in Fig. 9. The details are referred to paper 2 of this thesis.

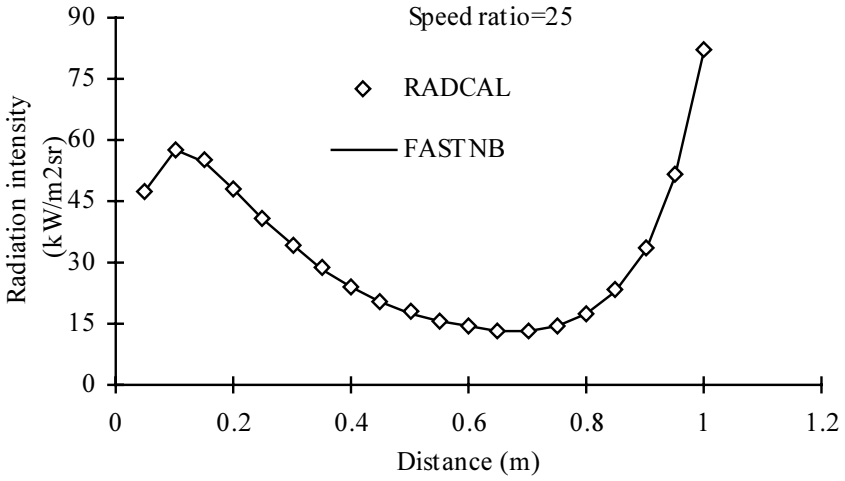

Fig. 9 Comparison of total intensities, for a path of parabolic minimum temperature and concentrations, with an even soot volume fraction of 2.0×10^{-6}. Note: speed ratio is defined as the CPU time required by RADCAL over the CPU time required by FASTNB.

(7) Integral model

With verified spectral data, the spectral narrow band method provides the best engineering accuracy and applicability for radiation property evaluation. For a simple isothermal and homogeneous path, based on curve-fitting, integral methods [75-78] are also available to estimate the total emissivity and absorptivity of H2O, CO2 and soot. The method proposed by Modak is employed in this work and will be briefly presented below.

The total radiation properties of soot can be obtained directly from integration of its spectral absorption coefficient. Assuming the complex refractive index, $m = n - ik$, is independent of the wavenumber, for a constant parameter path of length l, the absorptivity of soot is given by [78]

$$a_s = 1 - \frac{15}{\pi^4}\psi^{(3)}\left(1 + \frac{6\pi f_v \Im\left(\frac{m^2-1}{m^2+2}\right) T_s l}{c_2}\right) \tag{53}$$

where $\psi^{(3)}$ is the pentagamma function, T_s is the radiation source temperature and c_2 is the Planck's second constant.

The total emissivity of an individual gas (CO2 or H2O) is approximated in the form $\varepsilon(T_g, p_a, pl)$, using curve-fits based on three main parameters: temperature T_g, partial pressure p_a and pressure path-length pl. The emissivity of the mixture of CO2 and H2O is then estimated from

$$\varepsilon_{gas} = \varepsilon_{CO_2} + \varepsilon_{H_2O} - \Delta\varepsilon_{CO_2,H_2O} \tag{54}$$

where $\Delta\varepsilon_{CO_2,H_2O}$ accounts for the correction of the radiation overlapping of CO2 and H2O using the temperature-adjusted version of the approximate method proposed by Leckner [77, 79]

$$\Delta\varepsilon_{CO_2,H_2O} = \left\{\log_{10}\left[101.3(p_{H_2O} + p_{CO_2})l\right]\right\}^{2.76} F(P)F(T) \quad \text{if } (p_{H_2O} + p_{CO_2})l \geq 0.1 \ atm \cdot m \tag{55}$$

$$\Delta\varepsilon_{CO_2,H_2O} = 0 \quad \text{if } (p_{H_2O} + p_{CO_2})l < 0.1 \ atm \cdot m \tag{56}$$

where

$$F(P) = \frac{p_{H_2O}/(p_{H_2O} + p_{CO_2})}{10.7 + 101 p_{H_2O}/(p_{H_2O} + p_{CO_2})} - \frac{(p_{H_2O}/(p_{H_2O} + p_{CO_2}))^{10.4}}{111.7} \tag{57}$$

and

$$F(T) = -1.0204\times10^{-6}T^2 + 2.2449\times10^{-3}T - 0.23469 \quad (T \text{ in } K) \tag{58}$$

The absorptivity of the mixture of CO2 and H2O is approximated as

$$a_{gas} = \varepsilon_{gas}\left(\frac{T_g}{T_s}\right)^{(0.65 - 0.2 p_{H_2O}/(p_{H_2O} + p_{CO_2}))} \tag{59}$$

where ε_{gas} is the emissivity of an effective path length, $\frac{T_s}{T_g} l$, of the mixture of CO2 and H2O at temperature T_s.

The absorptivity of the mixture of soot, CO2 and H2O can be finally calculated by

$$a = a_s + a_{gas} - a_s a_{gas} \tag{60}$$

It should be noted that an unknown error could be introduced if the integral method is applied outside the range of its validity, such as to a non-isothermal and non-homogeneous path.

3.2 Modeling of the Response of Solid Material

The solid material responds and feeds back to the state variation of its surrounding gases. In a combustion system, which may experience drastic change in state, the processes happening inside the presented solid materials and the interaction between gas and solid phases must properly be considered. The most important processes inside a combustible solid material include heat conduction and pyrolysis, which will be discussed in the following.

3.2.1 Heat conduction inside a solid wall

Heat conduction inside a wall determines the internal temperature distribution and provides the necessary boundary condition for the gas phase calculation. For an inert wall, the heat balance is described by the following transient heat conduction equation

$$\frac{\partial(\rho H)}{\partial t} = \nabla \bullet (k \nabla T) \tag{61}$$

where H is the enthalpy given by $H = H_0 + \int_{T_0}^{T} c_p dT$. The specific heat c_p and conductivity k are usually temperature dependent and can be represented by polynomial functions.

When a solid wall is exposed to a flame, the heat conduction along the perpendicular wall surface direction usually dominates. For simplicity, the problem can be reduced to be one-dimensional. Correspondingly, the multidimensional heat conduction equation reduces to its one-dimensional form, which is

$$\frac{\partial(\rho H)}{\partial t} = \frac{\partial}{\partial x}(k \frac{\partial T}{\partial x}) \tag{62}$$

The initial and boundary conditions can be given by

$$T(t = 0, x) = T_0(x) \tag{63}$$

$$k \frac{\partial T}{\partial x}\Big|_{surface} = h_c (T_{gas} - T_{surface}) + R_{flux} \tag{64}$$

where R_{flux} represents the net radiation flux, T_{gas} is the temperature of the gas close to the wall surface and h_c is the convection heat transfer coefficient. These parameters are provided by the gas phase modeling of turbulent combustion.

The accuracy requirement of the numerical solution of this heat conduction equation necessitates adoption of a grid which can be much finer than that used in the gas phase computation. Therefore, a separate grid system is employed in the solid phase calculation. In the simplified one-dimensional case, the surface of a wall is subdivided into many small elements according to the gas phase grid, and along the direction which is perpendicular to the surface, each element is represented by a number of thin slices, which can be less than 1 mm thick.

3.2.2 Pyrolysis modeling

The detailed pyrolysis modeling of solid fuels is a very difficult task since the pyrolysis is usually highly complex.

For most combustible solid materials, the activation energy of the pyrolysis is large [80]. Due to the large activation energy and the endothermic feature of the pyrolysis process, the pyrolysis mainly happens in a narrow temperature range. The approximate constancy of the pyrolysis temperature suggests that below the pyrolysis temperature T , the pyrolysis reaction proceeds at negligible rate, but above the pyrolysis temperature, the chemistry becomes so fast that the pyrolysis rate is then essentially determined by the physical heat transfer. Therefore, as far as the mass release rate is concerned, the pyrolysis can well be described by the heat balance without the need of going to the detail of chemical reaction rates which will likely involve many unknown chemical mechanism parameters.

The pyrolysis reaction can be described in a simplified form as

$$Virgin\ \ material \rightarrow Volatile\ \ products + Char$$

For a non-charring material, char will not be produced during the pyrolysis.

Since chemical reactions do not affect the total enthalpy in a reacting system, the one-dimensional equation of energy balance in a pyrolysing material can be written as

$$\frac{\partial(\rho_{vir}h_{vir} + \rho_{char}h_{char} + \rho_{vol}h_{vol})}{\partial t} + \frac{\partial(\dot{m}'' h_{vol})}{\partial x} = \frac{\partial}{\partial x}(k\frac{\partial T}{\partial x}) \tag{65}$$

where h is the total enthalpy and $\dot{m}''$ is the mass flux of the volatile products. The three terms in the above equation represent the energy storing, energy convection due to the flow of the volatile products and heat conduction, respectively. The effects of pressure variation and flow kinetic energy are ignored.

The mass continuity gives

$$\frac{\partial(\rho_{vir}+\rho_{char}+\rho_{vol})}{\partial t}+\frac{\partial \dot{m}''}{\partial x}=0 \tag{66}$$

For simplicity, we assume an instant escape of the volatile products from the solid. Thus, we have $\frac{\rho_{vol}}{\partial t}=0$ and $\rho_{vol}=0$. If we further write $\rho_{vir}+\rho_{char}$ as ρ_s and assume $h_{vir}=h_{char}=h_s$, where the subscript s denotes the solid, the above two equations can be rewritten as

$$\frac{\partial(\rho_s h_s)}{\partial t}+\frac{\partial(\dot{m}'' h_{vol})}{\partial x}=\frac{\partial}{\partial x}(k\frac{\partial T}{\partial x}) \tag{67}$$

$$\frac{\partial \rho_s}{\partial t}+\frac{\partial \dot{m}''}{\partial x}=0 \tag{68}$$

Combining Eqs. 67 and 68 gives

$$\frac{\partial\left[\rho_s(h_s-h_{s,0})\right]}{\partial t}+\frac{\partial\left[\dot{m}''(h_{vol}-h_{s,0})\right]}{\partial x}=\frac{\partial}{\partial x}(k\frac{\partial T}{\partial x}) \tag{69}$$

where $h_{s,0}$ is the total enthalpy of the solid at a reference temperature T_0 and $h_s-h_{s,0}$ is the sensible enthalpy given by $h_s-h_{s,0}=\int_{T_0}^{T}c_{p,s}dT$. For later convenience, we define $H_s=h_s-h_{s,0}=\int_{T_0}^{T}c_{p,s}dT$.

The total enthalpy of volatile products can be written as

$$h_{vol}=h_{s,T_p}+H_{py}+\int_{T_p}^{T}c_{p,vol}dT \tag{70}$$

where H_{py} is the chemical converting heat associated with unit mass of volatile products, and can be calculated by the difference in total enthalpy of virgin material and volatile products at temperature T_p, i.e.

$$H_{py}=h_{vol,T_p}-h_{s,T_p}=h_{vol,T_p}-h_{vir,T_p}=h_{vol,T_p}-(h_{vir,T_0}+\int_{T_0}^{T_p}c_{p,vir}dT) \tag{71}$$

It is worth pointing out that H_{pp} is approximately constant for a specific material and is different from the heat of gasification, H_g, where

$$H_g=\dot{q}_{net}/\dot{m}_{total}=\left[h_c(T_g-T_{x=0})+R_{flux}\right]/\dot{m}_{total} \tag{72}$$

which is a local and transient value and changes considerably during the pyrolysis process [81]. For the thermally thick vaporizing material, at steady state

$$H_g = h_{vol,T_p} - h_{vir,T_0} = H_{py} + \int_{T_0}^{T_p} c_{p,vir}\, dT \tag{73}$$

Assuming equal specific heats, Eq. 70 becomes

$$h_{vol} = h_s + H_{py} \tag{74}$$

and the l.h.s of Eq. 69 can be reorganized as

$$\begin{aligned}
&\frac{\partial\left[\rho_s(h_s - h_{s,0})\right]}{\partial t} + \frac{\partial\left[\dot{m}''(h_{vol} - h_{s,0})\right]}{\partial x} \\
&= \frac{\partial(\rho_s H_s)}{\partial t} + \frac{\partial\left[\dot{m}''(H_{py} + H_s)\right]}{\partial x} \\
&= \frac{\partial(\rho_s H_s)}{\partial t} + \frac{\partial\left[\dot{m}''(H_{py} + H_{T_p})\right]}{\partial x} + \frac{\partial\left[\dot{m}''(H_s - H_{T_p})\right]}{\partial x} \\
&= \frac{\partial(\rho_s H_s)}{\partial t} + \dot{m}'''(H_{py} + H_{T_p}) + \frac{\partial\left[\dot{m}''(H_s - H_{T_p})\right]}{\partial x}
\end{aligned} \tag{75}$$

where $\dot{m}''' = -\frac{\partial \rho_s}{\partial t} = \frac{\partial \dot{m}''}{\partial x} \geq 0$, representing the mass loss rate of the pyrolysing material per unit volume.

Since the pyrolysis happens in a narrow temperature range around T_p, we can therefore rewrite the above equation approximately as (for convenience, the subscript s will be dropped from ρ and H in the following)

$$\frac{\partial(\rho H)}{\partial t} + \dot{m}'''(H_{py} + H) + \frac{\partial\left[\dot{m}''(H_{vol} - H_{vol,T_p})\right]}{\partial x} = \frac{\partial}{\partial x}(k\frac{\partial T}{\partial x}) \tag{76}$$

where the third term is the energy required to heat the vaporised gas as it flows to the solid surface. This term has no important effect in this study, thus it is ignored here. But it can be very easily included.

Noting that $\frac{\partial(\rho H)}{\partial t} = H\frac{\partial \rho}{\partial t} + \rho\frac{\partial H}{\partial t} = H\frac{\partial \rho}{\partial t} + \rho c_p \frac{\partial T}{\partial t}$ and $\dot{m}''' = -\frac{\partial \rho}{\partial t}$, the above equation can be rewritten as

$$\rho c_p \frac{\partial T}{\partial t} + \dot{m}''' H_{py} = \frac{\partial}{\partial x}(k\frac{\partial T}{\partial x}) \tag{77}$$

Assumptions have been introduced during the derivation of the simplified energy conservation equation. These assumptions can be more justified for non-charring materials. To be more general, assumptions can be lifted at the expense of increasing the complexity.

As mentioned before, the pyrolysis rate is slow when the material temperature is below its pyrolysis temperature, T_p, and becomes fast when the temperature is above T_p. As an approximation, we can reasonably assume that:

- The material will start to pyrolyse only when its temperature reaches the pyrolysis temperature
- Once started, the endothermic pyrolysis process will adjust its rate to keep the material temperature at the pyrolysis temperature until the material is completely pyrolysed

Thus we have

$$\rho c_p \frac{\partial T}{\partial t} = \frac{\partial}{\partial x}(k \frac{\partial T}{\partial x}) \qquad \text{when } T \le T_p \text{ or } \rho \equiv \rho_{char} \tag{78}$$

$$\dot{m}''' H_{py} = \frac{\partial}{\partial x}(k \frac{\partial T}{\partial x}) \qquad \text{when } T \ge T_p \text{ and } \rho > \rho_{char} \tag{79}$$

To implement the numerical solution, Eq. 77 needs to be discretised first. Using the fully implicit backward time stepping and central space difference scheme, the discretised equation can be written as

$$\rho c_p \frac{T_n - T_n^{'}}{\Delta t} \delta x + \dot{m}_{\delta x}'' H_{py} = k_{(n+1)(n)} \frac{T_{n+1} - T_n}{\delta x} - k_{(n)(n-1)} \frac{T_n - T_{n-1}}{\delta x}) \tag{80}$$

where the prime indicates the previous time step, $\dot{m}_{\delta x}''$ is the mass loss rate per unit area of the δ_x thick strip, the footnote of the conductivity k denotes the two temperature nodes between which the surface of the control volume is located.

For convenience, we reorganize the discrete equation as

$$A_p T_n = A_e T_{n+1} + A_w T_{n-1} + S_u \tag{81}$$

where

$$A_e = \frac{k_{(n+1)(n)}}{\delta x}; \qquad A_w = \frac{k_{(n)(n-1)}}{\delta x} \tag{82}$$

$$A_p = A_e + A_w + \rho c_p \delta x / \Delta t; \tag{83}$$

$$S_u = \rho c_p \delta x T_n^{'} / \Delta t - \dot{m}_{\delta x}^{''} H_{py} \tag{84}$$

Since the conductivity, k, is generally a function of temperature, it may vary with x and it is not necessary for A_e to be equal to A_w.

The fully implicit difference will necessitate the numerical iteration. When the pyrolysis model is used at the stand-alone mode, one may avoid the iteration by employing a semi-implicit difference with some properties properly evaluated at previous time step, as presented in paper 7. However, the fully implicit procedure is preferred in flame spread simulations since the pyrolysis needs to be solved in an iterative fashion coupled with CFD computation due to the complex interaction between the gas and solid phases.

In order to get a reasonable result for the mass loss rate, a very fine grid was required to resolve the pyrolysing layer and locate the pyrolysis front. However, this very fine grid is unnecessary and very expensive for the temperature solution. This inconsistency is overcome by introducing a dual mesh concept where a relatively coarser grid is defined for temperature solution and then refined into a second grid for the mass loss rate calculation, as shown in Fig. 10.

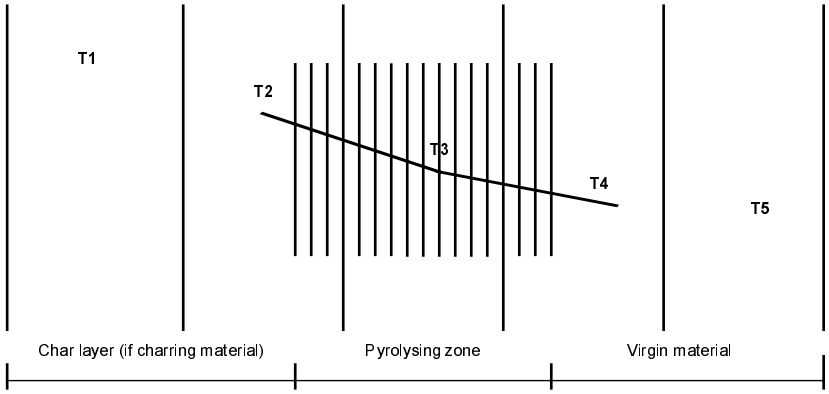

Fig. 10 Temperature solution grid and its refinement (Example with $N = 5$, $M = 10$, where N is the coarser grid number and M is the refined grid number in a coarser grid)

The temperature of the refined grid, m, of the coarser grid, n, (we will denote this grid as grid (n,m) later), $T_{n,m}$ is obtained by interpolation, as shown in Fig. 10, assuming a linear distribution between T_n and T_{n+1}.

During the iteration, $T_{n,m}$ may exceed the pyrolysis temperature. In and only in this case, the endothermic pyrolysis will be induced and then it will adjust itself to limit the local temperature to the pyrolysis temperature. Thus, from Eq. 81, for an arbitrary refined grid (n,m), the energy available for pyrolysis can be approximated as

$$H_{n,m} = \max\left[0.0, A_p(T_{n,m} - T_p)/M\right] \tag{85}$$

where M has been defined in Fig. 10.

The above energy excess allows the pyrolysing layer to spread over some numer of refined grids and provides one necessary, but not sufficient, factor to determine the pyrolysis rate.

In order to finally calculate the pyrolysis rate, one also needs to know the mass of the volatible material remaining in the refined grid (n,m). The volatible mass remaining in a refined grid can be easily calculated by monitoring its density history. However, this would require much memory storage, particularly when dealing with a large number of pyrolysing solid elements in flame spread simulations. In order to minimize the memory usage and make the data structure of the computer program more tidy, only the variation of the average density of the coarser grids is followed. The density of a refined grid is calculated by assuming a specific density distribution in the coarser grid. For a coarser grid of an average density which is equal to ρ_{char} or ρ_{vir}, the density of its refined grid will simply be the same as the average density. For a partly pyrolysed coarser grid, if we assume that the char layer and the virgin material is separated by a single partly pyrolysed refined grid, the density of a refined grid will be either ρ_r , ρ_{vir} or $\rho_{mix} = M\rho' - (m_0 - 1)\rho_{char} - (M - m_0)\rho_{vir}$. In the ρ_{mix} formula, ρ' is the average density of the coarser grid, the integer m_0 locates the assumed partly pyrolysed refined grid and can be determined by requiring $\rho' < \rho_{mix} < \rho_{vir}$.

For an arbitrary refined grid (n,m), the density can be generalized by a single formula

$$\rho_{n,m} = \min\left[\rho_{vir}, \max(\rho_{char}, \rho_{mix})\right] \tag{86}$$

By using the above formula, the value of the integer m_0 for the partly pyrolysed refined grid does not need to be explicitly calculated.

The mass of the volatizable material remaining in the grid (n,m) is given by

$$mass_{vol} = \frac{\delta x}{M}(\rho_{,m} - \rho_{char})$$

$$= \frac{\delta x}{M}\min\left\{\rho_{vir} - \rho_{char}, \max\left[0.0, (\rho_{mix} - \rho_{char})\right]\right\} \tag{87}$$

The mass loss rate from grid (n,m) is thus finally determined by

$$\dot{m}_{n,m} = \min\left\{H_{n,m}/H_{py}, mass_{vol}/\Delta t\right\} \tag{88}$$

The overall pyrolysis rate can be obtained by the summation over all the grids and expressed as

$$\dot{m} = \sum_n \sum_m \dot{m}_{n,m} = \sum_n \sum_m \min(H_{n,m} / H_{py}, mass_{vol} / \Delta t) \tag{89}$$

The corresponding heat release rate is represented by

$$\dot{Q} = \dot{m} H_c \tag{90}$$

where H_c is the heat of combustion related to the gaseous fuel produced. Generally, during flaming combustion, it has been shown that H_c is approximately constant [82].

As a basic test, the pyrolysis model was used successfully to simulate the Cone Calorimeter tests of both charring material (particle board) and non-charring material (PMMA). See paper 1 of this thesis for details.

This pyrolysis model is very fast and describes the essential physics, in so far as is needed to predict correct mass loss and heat release rates. It can easily be used in the complex cases such as those with transient incident heat flux and temperature dependent material properties. It is applicable to both charring and non-charring materials and can automatically consider the regression of the surface of the non-charring solid material during its pyrolysis.

Using this pyrolysis model, an "equivalent properties" optimization program can be developed to analyse and fit the Cone Calorimeter test results. A data base of the "equivalent properties" of the materials tested in the Cone can thus be created. By using the optimised equivalent properties, this pyrolysis model can be expected to be applicable to realistic composite materials and be used as an alternative to the more complex and expensive model [83]. Some recent advances in the optimization program development, which was initiated by J. deRis (FMRC, USA), is presented in paper 7 appended in this thesis.

4. INITIAL AND BOUNDARY CONDITIONS

When solving differential equation systems, initial and boundary conditions must be properly imposed. For a transient system, the initial condition provides the starting state of the system evolution. It can also be used in a steady system when the virtual time step is used as numerical relaxation. The specification of an initial condition is relatively simple. The initial condition is often specified with an idealization of the system or simply comes from a previous time step solution. The boundary condition provides the restrictive condition at the space coordinates for the differential equations. The most often used types include inlet, outlet, free, symmetry and wall boundary conditions. The wall boundary condition is normally the most complex one, and will thus be discussed in the following.

In a combustion system, the gas phase may have mass, momentum and energy exchanges with its solid boundaries. When the solid boundaries are inert (non-combustible), the mass exchange may not happen unless external surface mass injection is imposed. For a combustible solid boundary, the mass exchange mainly represents the release of gas components from the solid boundary resulting from its pyrolysis process. As a chemical sink and source, the surface combustion such as char burning also induces mass exchange. One important momentum exchange mechanism between solid and gas phases is the gas viscosity. The solid boundary is usually assumed to be non-slip. This momentum exchange is important for the gas flow, but has no important effect on a large solid boundary. The energy exchange includes the heat transfer through both radiation and convection. The radiation is a long distance transfer and has been discussed earlier. The convection is closely related to the local boundary layer profile. All these exchanges are strongly coupled. The release of gas component from a solid boundary into the boundary layer will create a blowing effect, which alters the boundary profile and thus affects the viscous shear stress on the solid surface and the convection heat transfer. Both the surface viscous shear stress and the convection heat transfer are dependent on the boundary layer development, and thus coupled. As discussed earlier, the rate of the mass release resulting from the pyrolysis of the combustible solid boundary is strongly dependent on the heat transfer. The mass release and pyrolysis of the combustible solid boundary has been discussed in a previous section. The following section describes the viscous momentum exchange and convective heat transfer in the boundary layer with blowing effect.

The boundary layer is normally a thin region of high gradients of dependent variables. If extensive heat transfer is present, the transport properties may also experience sharp variations across this thin layer. Furthermore, many two-equation turbulence models, including the high Reynolds number $k-\varepsilon$ model, fail in the region close to the wall [26]. The high Reynolds number $k-\varepsilon$ model is only valid in the region of fully turbulent flows, where the turbulent viscosity dominates over the laminar one. As a result, the boundary layer needs some special treatments. To cope with the turbulent boundary layer, one may in principle, numerically resolve the whole boundary layer with a proper consideration of low Reynolds number effect, or use an analytical approximation of the boundary layer profile to deviate the integration over the viscous sublayer.

When using the high Reynolds number $k-\varepsilon$ model in the computation, for simplicity and efficiency, the approximation termed wall function is normally adopted to provide for the computation the boundary conditions at the solid boundaries. Due to the reasons discussed above, the grid points where the wall function boundary conditions will be applied should be sufficiently far away from the wall surface.

For a stationary two dimensional boundary layer, with the absent of pressure gradient and surface mass injection, the following relations exist in the log layer where the laminar viscosity and convection can be ignored

$$u_+ = \frac{1}{\kappa}\ln(Ey_+) \tag{91}$$

where $u_+ = \frac{u}{u_\tau} = \frac{u}{\sqrt{\tau_w/\rho}} = \frac{u}{\sqrt{\nu(\frac{\partial u}{\partial y})_{y=0}}}$, u represents the mean velocity, $y_+ = \frac{u_\tau y}{\nu}$ and is a Reynolds number based on the friction velocity and the node distance from the wall surface, κ is the Karman constant of about 0.42 and E is an integration constant of about 9.7. Since the shear stress is approximately constant across the log layer and the viscous sublayer, $\tau_w = \left[\rho\nu(\frac{\partial u}{\partial y})\right]_{y=0} \approx \tau = (\mu+\mu_t)\frac{\partial u}{\partial y}$.

Assuming a local equilibrium in the log layer, where the turbulence kinetic energy production is balanced by the dissipation, one can write

$$\mu_t(\frac{\partial u}{\partial y})^2 = \rho\varepsilon = \rho c_\mu k/(l/k^{0.5}) \tag{92}$$

Multiplying $\mu_t = \rho k^{0.5} l$ on both sides of the above equation yields

$$\tau = \mu_t\frac{\partial u}{\partial y} = c_\mu^{0.5}\rho k \tag{93}$$

This local equilibrium relation was also historically used to provide the model constant c_μ from experimental data.

Using Eq. 93, we can rewrite u_+ and y_+ as

$$u_+ = \frac{u}{c_\mu^{0.25}k^{0.5}} \tag{94}$$

$$y_+ = \frac{c_\mu^{0.25} k^{0.5} y}{\nu} \tag{95}$$

From the definition of u_+ and y_+, one can write

$$\tau = \frac{u y_+}{u_+ y} \mu \tag{96}$$

Combination of Eqs. 94-96 gives

$$\tau = \frac{\rho c_\mu^{0.25} k^{0.5} u}{u_+} \tag{97}$$

The boundary layer solution for a conserved scalar can be written as [84, 85]

$$\varphi_+ = \sigma_t \left(u_+ + P_e \right) \tag{98}$$

where φ_+ is defined as $\varphi_+ = (\varphi - \varphi_w)\sqrt{\rho \tau_w} / (-J_{\varphi,w})$, $J_{\varphi,w}$ is the scalar diffusion flux given by $J_{\varphi,w} = -\frac{\mu}{\sigma}\frac{\partial \varphi}{\partial y}$ and P_e can be considered as an integration constant.

When the surface mass injection is present, the blowing effect needs to be included in the above non-dimensional relations. If we define the non-dimensional mass injection parameter as $m_+ = \dot{m}_w'' / \sqrt{\rho \tau_w}$, then we have [84, 85]

$$u_+ = \kappa^{-1} \ln(E y_+) + (2\kappa)^{-2} m_+ \left[\ln(E y_+) \right]^2 \tag{99}$$

$$\varphi_+ = \left\{ \exp\left[\sigma_t \left(\ln(1 + m_+ u_+) + m_+ P_e \right) \right] - 1 \right\} / m_+ \tag{100}$$

The above formulas will need to take the laminar forms once the local point turns out to be located in the viscous sublayer. Their laminar forms are simply given here

If $m_+ \neq 0$:

$$u_+ = \left(\exp(m_+ y_+) - 1 \right) / m_+ \tag{101}$$

$$\varphi_+ = \left(\exp(\sigma_\varphi m_+ y_+) - 1 \right) / m_+ \tag{102}$$

If $m_+ = 0$:

$$u_+ = y_+ \tag{103}$$

$$\varphi_+ = \sigma_\varphi y_+ \tag{104}$$

Obviously, the formulas for $m_+ \neq 0$ will reduce correspondingly to those for $m_+ = 0$ at the limit $m_+ = 0$.

The turbulence kinetic energy dissipation rate can be calculated from kinetic energy cascade as [45]

$$\varepsilon = c_\mu k/(l/k^{0.5}) = c_\mu k^{1.5}/l \tag{105}$$

In the above equation, l is identified as the turbulence length scale used in the one equation turbulence model. In the boundary layer, this length scale can be obtained from the product of $c_\mu^{0.25}$ and the mixing length scale which can be given by $l_{mix} = \kappa y$. Therefore, we have

$$\varepsilon = c_\mu k/(l/k^{0.5}) = c_\mu^{0.75} k^{1.5}/(\kappa y) \tag{106}$$

The turbulence kinetic energy can be calculated from Eq. 93 or by solving the turbulence kinetic energy transport equation with the diffusion to the wall assumed zero and production modeled as $\int_V P dv \approx \tau_w \frac{u}{y} \cdot volume$ [86].

When the pressure gradient is present, the formulae will need to be modified and become more complex. In a combustion system, where the chemical reaction and radiation heat transfer may need to be considered in the boundary layer, the problem can quickly become intractable.

5. NUMERICAL SOLUTION

This section briefly discusses the mathematical aspects on seeking the numerical solution of the differential equations system established in the previous sections. Although it is extremely difficult to have a strict mathematical proof, it is believed that the solution exists and is unique.

The numerical solution is presented on a finite number of discrete points/elements with regard to both the time and space coordinates. Thus, the differential equations are applied to each discrete point/element and transformed into algebraic equations, which can be solved using an algebraic equation solver. When the geometry of the physical computation domain is complex, in order to ease the implementation of the boundary conditions, one may discrete the physical space using curvilinear coordinates system so that the boundary is located on a surface where one corresponding coordinate is constant. That is, the complex domain in physical space will be mapped onto a simple domain in computational space using coordinate transformation. In this case, the discretization of the differential equation can be proceeded by applying the differential transport equations directly to each of the general distorted control volumes, or transforming the equations from physical space to the computational space and then performing the discretization on the computational space. The above procedure will be explained in more detail in the following.

5.1 Coordinate Transformation

The transformation from Cartesian coordinate $x^i(x^1,x^2,x^3)$ to a general coordinate $\xi^i(\xi,\eta,\zeta)$ can be achieved either analytically or numerically. The analytical transformation can be used if the geometry is relatively simple, for example, in a cylindrical system. The numerical transformation generates the grid by solving algebraic or differential equations.

Assuming a non-singular transformation $\xi^i(x^i)$, the chain rule gives

$$\frac{\partial \varphi}{\partial x^i} = \frac{\partial \varphi}{\partial \xi^j}\frac{\partial \xi^j}{\partial x^i} = e_i^j \frac{\partial \varphi}{\partial \xi^j} \tag{107}$$

$$\frac{\partial \varphi}{\partial \xi^i} = \frac{\partial \varphi}{\partial x^j}\frac{\partial x^j}{\partial \xi^i} = e_{i(j)} \frac{\partial \varphi}{\partial x^j} \tag{108}$$

where e_i^j and $e_{i(j)}$ are the *ith* and *jth* Cartesian components of the contravariant and covariant frames of the basis vectors, respectively.

The above two formulas provide the basic aspects for the equation transformation. In principle, using these two formulas, all the physical space derivatives can be replaced by the computational space derivatives. However, this method does not show to be handy. The procedure can become simpler when using tensor analysis, as described below.

If we write the differential transport equation in a general form $\nabla \bullet (\rho \vec{V} \varphi - \mu_{eff} \nabla \varphi) = S$, then the elemental task in the transformation of the transport equations is to express the gradient and divergence properly in the computational space. For later convenience, we denote $g^{ij} = e^i \bullet e^j$, $g_{ij} = e_i \bullet e_j$ and $g = \det(g_{ij})$, which are related to the area vectors and volume of the parallelepiped generated by the triad e_i by

$$A^i = \frac{1}{2} \varepsilon_{ijk} e_j \times e_k = volume * e^i \tag{109}$$

$$\sqrt{g} = volume \tag{110}$$

$$volume = abs(e_i \bullet (e_j \times e_k)) \qquad (i \neq j \neq k) \tag{111}$$

where ε_{ijk} is the permutation tensor.

With these notations, in the computational space, the gradient and divergence are given by

$$\nabla \varphi = g^{ij} \frac{\partial \varphi}{\partial \xi^j} e_i \qquad \text{(for a general scalar } \varphi\text{)} \tag{112}$$

$$\nabla \bullet \vec{R} = \frac{1}{\sqrt{g}} \frac{\partial}{\partial \xi^i} (\sqrt{g} R^i) \qquad \text{(for a general vector } \vec{R} = R^i e_i\text{)} \tag{113}$$

As a result, the general form of the transport equations can be written as

$$\frac{1}{\sqrt{g}} \frac{\partial}{\partial \xi^i} (\sqrt{g} \rho V^i \varphi - \sqrt{g} g^{ij} \mu \frac{\partial \varphi}{\partial \xi^j}) = S \tag{114}$$

which can be easily discretised in the computational space by integrating the above equation over the control volumes.

The discretised equations in a general coordinate system can also be obtained by directly integrating the governing equations over each of the finite volumes in physical space.

5.2 Discretization and Solution

In order to obtain the solution using the current digital computer which can basically perform the simple standard mathematical and logical operations, the governing equations must be discretised in a general four-dimensional computational domain. The discretization can be carried out by finite difference, finite volume and spectral methods. The finite difference and finite volume methods are the commonly used methods, where the governing equations are applied to a set of representative

points and elementary volumes, respectively. With an assumption of proper temporal and spatial distributions of the dependent variables, the discretization transforms the general integral differential equations into algebraic equations, which relate the state of the central points/elements to those of neighboring points/elements. Since one has much freedom to choose different variable distributions, different numerical schemes can be adopted. The choice of numerical schemes is largely dependent on the numerical stability and accuracy. The commonly used schemes include fully explicit, fully implicit, Crank-Nicolson and Runge-Kutta methods in time, upwind, central, hybrid, power law and quadratic upwind schemes, etc., in space [45, 87-91]. In order to minimize the numerical error, high order schemes should be used when necessary [92-94].

The discretization procedure results in a set of algebraic equations, which can be solved using algebraic solvers. Simplicity and efficiency are the critical factors to be considered when selecting a proper numerical solver. For a small set of linear equations, a direct method may have its advantage. The iteration method is required when the equation is non-linear, and preferred in the applications which involve a large set of equations. The widely adopted solution methods are the Gauss-Seidel iteration method [87], the line-by-line tridiagonal matrix algorithm (TDMA) [45, 88], the strongly implicit procedure (SIP) [95] and the alternating direction implicit method (ADI) [96].

5.3 Coupling between Velocity and Pressure

The pressure gradient term appearing in the momentum equations creates a strong coupling between the pressure and velocity. A pressure difference, which can be very small compared to the absolute value of the pressure itself, can result in a large variation in the velocity. This strong coupling requires extra consideration during the numerical computation. The pressure correction methods, including SIMPLE (Semi-Implicit Method for Pressure-Linked Equations) [45, 88] and its variants such as the iterative PISO (Pressure-Implicit with Splitting of Operators) [97, 98], are widely used to deal with this strong coupling. In the pressure correction methods, approximate functions relating velocity corrections to pressure corrections are derived from momentum equations, and then substituted into the continuity equation to obtain the pressure correction equation which can be numerically solved as a usual scalar transport equation. Subsequently, pressure is updated and velocity is corrected according to the pressure correction. This procedure is repeated until convergence is reached.

In a general curvilinear coordinate system, a non-staggered grid system is usually adopted where velocity components and scalars are all defined at the same center of the control volume. In this case, the discretised momentum equation using $2\delta\xi$ centered pressure difference for the pressure gradient is insensitive to the $1\delta\xi$ pressure variation. This may create chequerboard oscillations in the pressure and velocity [99]. In order to remedy this problem, Rhie and Chow [99] proposed a simple and effective interpolation method, which ensures a strong velocity-pressure coupling.

6. CFD SIMULATION OF FLAME SPREAD

CFD simulation of flame spread is a comprehensive study, in which the essential knowledge of all the aspects mentioned above is necessary, but by no means sufficient. Within the simulation, all the important sub-processes must be properly considered.

In this thesis, attempts have been made to simulate the flame spread in room corner fires, in both 1/3 and full scale scenarios. The predicted flame spread pattern and heat release history in the 1/3 scale scenario are shown and compared with experimental measurements in Figs. 11 and 12. The detail of this study is referred to the appended paper 1.

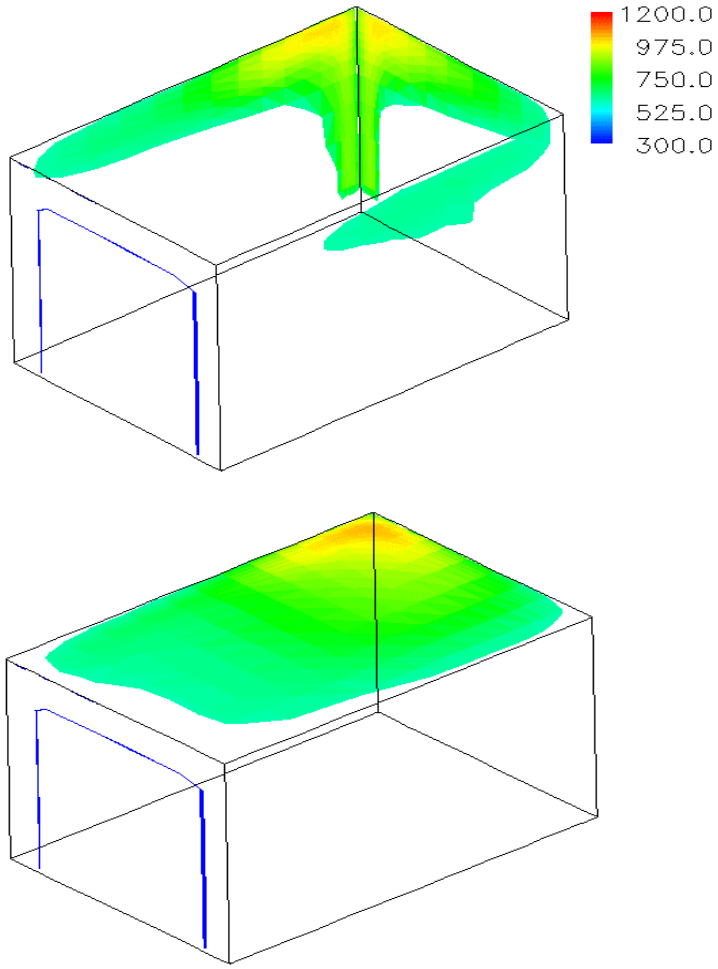

Fig. 11 Flame spread pattern in the 1/3 scale scenario, indicated by surface temperature (in K). (t=300s, threshold=600 K)

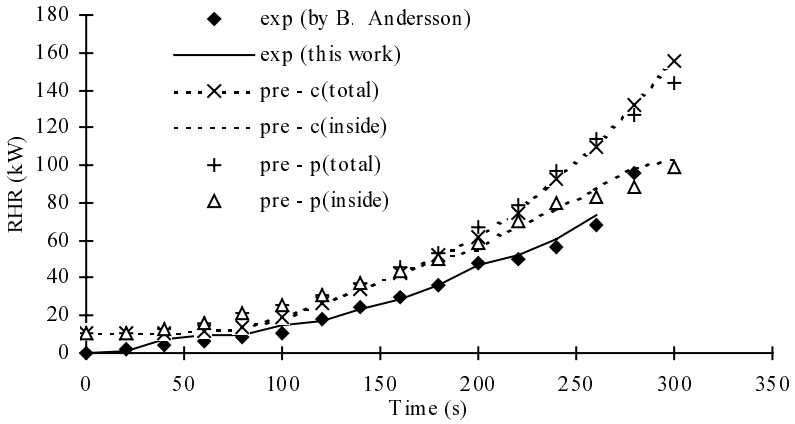

Fig.12 Calculated and measured heat release rates in the 1/3 scale scenario. The symbol (c) denotes using Cone data input method and (p) the pyrolysis model.

As expected, the predicted flame spread is sensitive to the heat flux. Considering the complexity of the physical problem, this would necessitate further extensive development and validation of CFD models.

7. BRIEF SUMMARY OF PAPERS

Paper 1

This paper includes both model development and application study.

A simple and promising model was developed to describe the pyrolysis of solid fuels. It considers the essential physics in so far as needed to correctly predict the mass release rate. A moving dual mesh method was developed and implemented in this pyrolysis model to provide the important high efficiency. This pyrolysis model was tested successfully against the experimental data for both charring and non-charring materials.

Comprehensive CFD simulations of both full and one-third scale room corner fire growths on particle board were carried out. To provide additional data for comparison, corresponding experimental tests on one-third scale room corner fire growth were performed to measure heat release rate, gas and surface temperature, radiation heat flux and char depth.

The CFD simulations were compared with experimental measurements. The results are reasonable and the comparison between prediction and experiment is fairly good and promising.

Paper 2

This paper presents model development.

A fast narrow band computer model, FASTNB, has been developed to speed up the evaluation of the radiation properties of a radiating medium in a general non-isothermal and non-homogeneous path, This provides a potential of applying the narrow band model in numerical simulations of practical turbulent combustion. Compared with Grosshandler's narrow band model, RADCAL, which has been verified quite extensively against experimental measurements, FASTNB is more than 20 times faster and gives almost exactly the same results.

Paper 3

This paper presents an application study.

Two-dimensional upward flame spread and subsequent steady burning of a vertical PMMA surface was studied using CFD methodology, with the following models employed and compared:

- Standard buoyancy modified $k-\varepsilon$ model

- EDC combustion model
- DT radiation model
- FASTNB radiation property evaluation model and an integral radiation property model
- Transpired and non-transpired wall functions
- Pyrolysis model (developed in paper 1)
- Empirical soot model

The calculated flame spread velocity, heat fluxes (including both convection and radiation), and the steady burning rate, etc. were analysed and compared with experimental measurements. Good agreement was obtained.

Paper 4

This paper presents an application study.

The heat transfer from turbulent diffusion flames between vertical walls has been computed for different wall and burner configurations. The following models were employed:

- Standard buoyancy modified $k-\varepsilon$ model
- Flamelet combustion model
- DT radiation model
- FASTNB radiation property evaluation model
- Two-parameter soot model proposed by Lindstedt

The results were analysed and compared with experimental measurements, with which they showed good agreement. The effects of wall separation and burner output on heat transfer were faithfully reproduced.

Paper 5

This paper presents a model development.

A modified $k-\varepsilon$ two-equation turbulence model was developed to improve the consideration of the important buoyancy effect on turbulence and turbulent transport, which is a serious deficiency of the standard buoyancy-modified $k-\varepsilon$ model. The present model was tested against both plane and axisymmetric thermal plumes and a buoyant diffusion flame. The model was found to be stable, computationally economic, promising and applicable to complex situations. The predicted plume spreading rates and velocity and temperature profiles agreed well with experimental measurements. When compared with the standard buoyancy-modified $k-\varepsilon$ turbulence model, this model gives significantly improved numerical results.

Paper 6

This paper presents an application study.

A number of numerical simulations of rack storage fires have been carried out, with various fuel types and burner outputs, with the following models adopted and compared:

- Standard buoyancy modified $k-\varepsilon$ model and a recent turbulence model (developed in paper 5)
- Flamelet combustion model
- DT radiation model
- FASTNB radiation property evaluation model
- Two-parameter soot model proposed by Lindstedt

The results, including heat flux and gas temperature profile, were analyzed and compared with experimental measurements. The comparisons showed considerably improved agreement for the new turbulence model.

Paper 7

This paper further presents the pyrolysis model originally developed by the author of this thesis in paper 1 and reports the progress towards the development of the "equivalent properties" optimization program using this pyrolysis model.

This model has been modified and coupled with MS Excel to provide a user-friendly interface for optimization process, mostly taking the advantage of its high efficiency.

As a further validation, it has also been used successfully to study how the sample ignition in Cone Calorimeter tests can be affected by the imposed heat flux, rear boundary condition and sample thickness, etc.

8. LIST OF NOT-INCLUDED PUBLICATIONS

1. Zhenghua Yan & Göran Holmstedt, CFD Simulation of Flame Spread in Room Fire, In First European Symposium on Fire Safety Science, pp. 95-96, 1995

2. Zhenghua Yan & Göran Holmstedt, Numerical Prediction of Heat Flux from Flame in Room Fire, Report 3090, Department of Fire Safety Engineering, Lund, 1997

3. Zhenghua Yan & Göran Holmstedt, Numerical Investigations of Rack Storage Fires, presented as poster in the 27th International Symposium on Combustion, Colorado, USA, 1998

4. Göran Holmstedt & Zhenghua Yan, CFD Simulation of Flame Spread and Pollution Formation in Room Fire, invited plenary lecture, CHEMECA 98, Australia, 1998

5. Petra Andersson, Sören Isaksson, Zhenghua Yan and Göran Holmstedt, Experimental Studies and CFD Simulations of a Fire Plume for the Prediction of Smoke Detector Activation, submitted to Fire Safety Journal

9. REFERENCES

1. D. Bradley, How Fast Can We Burn? 24th International Symposium on Combustion, The Combustion Institute, Pittsburgh, pp.247-262, 1992
2. T. Cebeci and A. M. O. Smith, Analysis of Turbulent Boundary Layers, Academic Press, 1974
3. H. Tennekes and J. L. Lumley, A First Course in Turbulence, The MIT Press, 1972
4. P. A. Libby, Introduction to Turbulence, Taylor & Francis, 1996
5. J. Sato, Effects of Lewis Number on Extinction Behavior of Premixed Flames in a Stagnation Flow, 19th International Symposium on Combustion, The Combustion Institute, Pittsburgh, pp.1541-1548, 1982
6. J. Sato and H. Tsuji, Extinction of Premixed Flames in a Stagnation Flow Considering General Lewis Number, Combustion Science and Technology, 33:193-205, 1983
7. N. Peters, Fifteen Lectures on Laminar and Turbulent Combustion, RWTH Aachen Ercoftac Summer School, Germany, 1992
8. A. N. Kolmogorov, A Refinement of Previous Hypotheses Concerning the Local Structure of Turbulence in a Viscous Incompressible Fluid at High Reynolds Number, J. Fluid Mech., 13:82-85, 1962
9. H. M. Oboukhov, Some Specific Features of Atmospheric Turbulence, J. Fluid Mech., 13:77-81, 1962
10. R. Borghi, In 'Recent Advances in the Aerospace Science', (C. Bruno and C. Casci, eds.), Plenum, New York, 1984
11. R. G. Adbel-Gayed, D. Bradley, and F. K.-K. Lung, Combustion Regimes and the Straining of Turbulent premixed Flames, Combustion and Flame, 76:213-218, 1989
12. B. F. Magnussen and B. H. Hjertager, On Mathematical Modeling of Turbulent Combustion with Special Emphasis on Soot Formation and Combustion, In 16th Symp. (Int.) on Combustion, The Combustion Institute, Pittsburgh, pp. 719-729, 1976
13. B. F. Magnussen, The Eddy Dissipation Concept, Presented at Task Leader Meeting, Lund, Sweden, 1989
14. F. A. Williams, Turbulent Mixing in Non-reactive and Reactive Flows (S. N. B. Murthy, ed.), pp.189, Plenum, 1975
15. S. K. Liew, Flamelet Models of Turbulent Non-premixed Combustion, Ph.D. thesis, University of Southampton, 1983
16. N. Peters, Laminar Diffusion Flamelet Model in Non-premixed Turbulent Combustion, Prog. Energy Combust. Sci., 10:319-339, 1984
17. S. K. Liew, K. N. C. Bray, and J. B. Moss, A Stretched Laminar Flamelet Model of Turbulent Non-premixed Combustion, Combust and Flame, 56:199-213, 1984

18. N. Peters, Laminar Flamelet Concepts in Turbulent Combustion, Twenty-first Symp. (International) on Combustion, The Combustion Institute, Pittsburgh, pp. 1231-1250, 1986
19. N. Peters, Four Lectures on Turbulent Combustion, ERCOFTAC Summer School, Aachen, Germany, 1997
20. J. B. Moss, In 'Combustion Fundamentals of Fire' (G. Cox, Ed.), Academic Press, pp. 221, 1995
21. F. A. Williams, Combustion Theory, Second Edition, The Benjamin/Cummings Publishing Company, Inc., Menlo Park, 1985
22. K. K. Kuo, Principles of Combustion, John Wiley & Sons Inc., New York, 1986
23. J. R. Andrews and O. Biblarz, Temperature Dependence of Gas Properties in Polynomial Form, Report NPS67-81-001, NAVA Postgraduate School Monterey, CA 93940, 1981
24. S-M. Jeng, M-C. Lai, and G. M. Faeth, Nonluminious Radiation in Turbulent Buoyant Axisymmetric Flames, Combustion Science and Technology, 40:41-53, 1984
25. S-M. Jeng, and G. M. Faeth, Radiative Heat Fluxes Near Turbulent Buoyant Methane Diffusion Flames, J. Heat Transfer, 106:886-888, 1984
26. D. C. Wilcox, Turbulence Modeling for CFD, DCW Industries Inc., 1993
27. N. N. Mansour, J. Kim, and P. Moin, Reynolds Stress and Dissipation Rate Budgets in Turbulent Channel Flow, Journal of Fluid Mechanics, 194:15-44, 1988
28. V. B. Librovich and V. I. Lisitzyn, AIAA J., 15, 227, 1977
29. M. A. Leschziner, Turbulence Modeling, Lecture Note, Summer School on Advanced Turbulence Modeling, Udine, Italy, 1998
30. M. O. Annarumma, J. M. Most and P. Joulain, On the Numerical Modeling of Buoyant-Dominated Turbulent Vertical Diffusion Flames, Combustion and Flame, 85:403-415, 1991
31. S. Nam and R. G. Bill, Numerical Simulation of Thermal Plumes, Fire Safety Journal, 21:231-256, 1993
32. P. Woodburn, Computational Fluid Dynamics Simulation of Fire-generated Flows in Tunnels and Corridors, Ph.D. thesis, University of Cambridge, 1995
33. W. C. Strahle, Duality, Dilatation, Diffusion and Dissipation in Reacting Turbulent Flows, 19th International Symposium on Combustion, The Combustion Institute, Pittsburgh, pp.337-347, 1982
34. R. E. Mitchell, A. F. Sarofim and L. A. Clomburg, Experimental and Numerical Investigation of Confined Laminar Diffusion Flames, Combustion and Flame, 37:227-244, 1980
35. Y. R. Sivathanu and G. M. Faeth, Generalized State Relationships for Scalar Properties in Nonpremixed Hydrocarbon/Air Flames, Combustion and Flame, 82:211-230, 1990
36. H. Tsuji and I. Yamaoka, The Structure of Counterflow Diffusion Flames in The Forward Stagnation Region of a Porous Cylinder, 12th International Symposium on Combustion, The Combustion Institute, Pittsburgh, pp.997-1005, 1968

37. N. Peters and R. J. Kee, The Computation of Stretch Laminar Methane-Air Diffusion Flames Using a Reduced Four-Step Mechanism, Combustion and Flame, 68:17-29, 1987

38. W. P. Jones and R. P. Lindstedt, The Calculation of the Structure of Laiminar Counterflow Diffusion Flames Using a Global Reaction Mechanism, Combustion Science and Technology, 61:31-49, 1988

39. H. Pitsch and N. Peters, A Consistent Flamelet Formulation for Non-premixed Combustion Considering Differential Diffusion Effects, Combustion and Flame, 114:26-40, 1998

40. S. B. Pope, The Probability Approach to the Modelling of Turbulent Reacting Flows, Combustion and Flame, 27: 299-312, 1976

41. S. B. Pope, Monte Carlo Calculation of Premixed Turbulent Flames, Eighteenth Symposium on Combustion, The Combustion Institute, Pittsburgh, pp.1001-1010, 1981

42. S. B. Pope, A Monte Carlo Method for the PDF Equations of Turbulent Reactive Flow, Combustion Science and Technology, 25:159-174, 1981

43. W. P. Jones and M. Kakhi, Pdf Modeling of Finite-rate Chemistry Effects in Turbulent Nonpremixed Jet Flames, Combustion and Flame, 115:210-229, 1998

44. F. C. Lockwood and A. S. Naguib, The Prediction of the Fluctuations in the Properties of Free, Round-jet, Turbulent, Diffusion Flames, Combustion and Flame, 24:109-124, 1975

45. W. C. Fan, Y. L. Chen and M. L. Hong, Computational Combustion, Anhui Academic Press, 1985

46. Y. P. Wan, H. Pitsch and N. Peters, Simulation of Autoignition Delay and Location of Fuel Sprays Under Diesel-Engine Relevant Conditions, SAE 971590, 1997

47. H. Pitsch, Y. P. Wan and N. Peters, Numerical Investigation of Soot Formation and Oxidation Under Diesel Engine Conditions, SAE 952357, 1995

48. H. Pitsch, H. Barths and N. Peters, Three-Dimension Modeling of NOx and Soot Formation in DI Diesel Engine Using Detailed Chemistry Based on the Interactive Flamelets Approach, SAE 962057, 1996

49. I. Glassman, Soot Formation in Combustion Processes, Twenty Second International Symposium on Combustion, The Combustion Institute, Pittsburgh, pp.295-311, 1988

50. I. Glassman, Combustion, Third Edition, Academic Press, San Diego, 1996

51. H. Bockhorn (Ed.), Soot Formation in Combustion - Mechanisms and Models, Springer-Verlag, 1994

52. J. B. Moss, C. D. Stewart, and K. J. Syed, Flowfield Modeling of Soot Formation at Eleveted Pressure, Twenty-Second Symposium (International) on Combustion, The Combustion Institute, Pittsburgh, pp. 413-423, 1988

53. K. J. Syed, C. D. Stewart, and J. B. Moss, Modeling Soot Formation and Thermal Radiation in Buoyant Turbulent Diffusion Flames, Twenty-Third Symposium (International) on Combustion, The Combustion Institute, Pittsburgh, pp. 1533-1541, 1990

54. C. D. Stewart, K. J. Syed, and J. B. Moss, Modeling Soot Formation in Non-premixed Kerosine-Air Flames, Combustion Science and Technology, 75:211-226, 1991

55. J. B. Moss, C. D. Stewart, and K. J. Young, Modeling Soot Formation and Burnout in a High Temperature Laminar Diffusion Flame Burning Under oxygen-Enriched Conditions, Combustion and Flame, 101:491-500, 1995

56. R. P. Lindstedt, Invited Lecture, 1st Specialist Meeting of the International Flame Research Foundation, Ijmuijden, October, 1989

57. R. P. Lindstedt, A Simple Reaction Mechanism for Soot Formation in Non-premixed Flames, IUTAM Conference on Aerothermo-chemistry in Combustors, Taipei, Taiwan, June 1991

58. M. Fairweather, W. P. Jones, H. S. Ledin, and R. P. Lindstedt, Prediction of Soot Formation in Turbulent Non-premixed Propane Flames, Twenty-Fourth Symposium (International) on Combustion, The Combustion Institute, Pittsburgh, pp. 1067-1074, 1992

59. M. Fairweather, W. P. Jones, and R. P. Lindstedt, Predictions of Radiative Transfer from a Turbulent-Reacting Jet in a Cross-Wind, Combustion and Flame, 89:45-63, 1992

60. M. Balthasar, A. Heyl, F. Mauss, F. Schmitt, and H. Bockhorn, Flamelet Modeling of Soot Formation in Laminar Ethyne/Air Diffusion Flames, Twenty-Sixth Symposium (International) on Combustion, The Combustion Institute, Pittsburgh, pp. 2369-2377, 1996

61. R. Siegel and J. R. Howell, Thermal Radiation Heat Transfer, Hemisphere Publishing Corp., Washington, 1992

62. M. F. Modest, Radiative Heat Transfer, McGraw-Hill, Inc., New York, 1993

63. F. C. Lockwood & N. G. Shah, A New Radiation Solution Method for Incorporation in General Combustion Prediction Procedures, Eighteenth Symposium (International) on Combustion, The Combustion Institute, Pittsburgh, pp. 1405-1414, 1981

64. M. A. Heaslet and R. F. Warming, Radiative Transport and Wall Temperature Slip in an Absorbing Planar Medium, Int. J. Heat Mass Transfer, 8:979-994, 1965

65. S. S. Dua and P. Cheng, Multi-dimensional Radiative Transfer in Non-isothermal Cylinderical Media with Non-isothermal Bounding Walls, Int. J. Heat Mass Transfer, 18:246-259, 1975

66. H. C. Hottel and A. F. Sarofim, Radiative Transfer, McGraw-Hill, New York, 1967

67. D. K. Edwards and A. Balakrishnan, Thermal Radiation by Combustion Gases, Int. J. Heat Mass Transfer, 16:25-40, 1973

68. C. Ludwig, W. Malkmus, J. Reardon and J. Thomson, Handbook of Infrared Radiation from Combustion Gases, NASA SP-3080, 1973

69. W. Ranz, and W. Marshall, Chem. Eng. Progr., 48, 141, 1952

70. J. deRis, Fire Radiation - A Review, 17th Int. Symposium on Combustion, The Combustion Institute, Pittsburgh, pp.1003-1016, 1978

71. J. deRis and R. L. Alpert, Prediction of Fire Dynamics-Final and Fourth Quarterly Report, Factory Mutual Research Corporation, 1993

72. M. A. Brosmer and C. L. Tien, Thermal Radiation Properties of Propylene, Comb. Sci. and Tech., 48:163-175, 1986

73. M. A. Brosmer and C. L. Tien, Thermal Radiation Properties of Acetylene, J. of Heat Transfer, 107:943-948, 1985

74. W. L. Grosshandler, RADCAL: A Narrow-Band Model for Radiation Calculation in a Combustion Environment, NIST technical note 1402, 1993

75. H. C. Hottel and R. B. Egbert, Radiant Heat Transmission from Water Vapor, American Institute of Chemical Engineers, Presented at Joint Symp. With the Heat Transfer Division of ASME at Boston, MIT, pp.531-565, 1942

76. H. C. Hottel and H. G. Mangelsdorf, Heat Transmission by Radiation from Non-luminous Gases II, Experimental Study of Carbon Dioxide and Water Vapor, American Institute of Chemical Engineers, pp.517-549, 1956

77. A. T. Modak, Radiation from Products of Combustion, Fire Research, 1:339-361, 1978/1979

78. J. D. Felske and C. L. Tien, Calculation of the Emissivity of Luminous Flames, Combustion Science and Technology, 7:25-31, 1973

79. B. Leckner, Spectral and Total Emissivity of Water Vapor and Carbon Dioxide, Combustion and Flame, 19:33-48, 1972

80. A. C. Fernandez-Pello, In 'Combustion Fundamentals of Fire', (G. Cox, Ed.), Academic Press, pp.31, 1995

81. M. Sibulkin, Heat of gasification for Pyrolysis of Charring Materials, Fire Safety Science-Proceeding of the First International Symposium, pp. 391-400, 1985

82. L. Tsantaridis & B. Östman, Smoke, Gas and Heat Release data for Building Products in the Cone Calorimeter, Report I 8903013, Trateknik Centrum, Sweden, 1989

83. B. Fredlund, A Model for Heat and Mass Transfer in Timber Structures During Fire, Ph.D. Thesis, Department of Fire Safety Engineering, Lund University, 1988

84. S. V. Patankar and D. B. Spalding, Heat and Mass Transfer in Boundary Layers, 2nd edition, International Textbook Company Ltd., 1970

85. D. B. Spalding, Genmix - A General Computer Program for Two Dimensional Parabolic Phenomena, Pergamon Press, 1977

86. B. E. Launder and D. B. Spalding, The Numerical Computation of Turbulent Flows, Computer Methods in Applied Mechanics and Engineering, 3:269-289, 1974

87. K. L. Guo, Numerical Heat Transfer, Anhui Academic Press, 1985

88. S. V. Patankar, Numerical Heat Transfer and Fluid Flow, Hemisphere, New York, 1980

89. R. Peyret, Introduction to High-Order Approximation Methods for Computational Fluid Dynamics, Lecture Note, Summer School on Advanced Turbulence Modeling, Udine, Italy, 1998

90. B. P. Leonard, A Stable and Accurate Convective Modeling Procedure Based on Quadratic Upstream Interpolation**,** Computer Methods in Applied Mechanics and Engineering, 19:59-98, 1979

91. R. W. Johnson and R. J. Mackinnon, Equivalent Versions of the QUICK Scheme for Finite-Difference and Finite-Volume Numerical Methods, Communications in Applied Numerical Methods, 8:841-847, 1992

92. F. Bade and P. Haldenwang, High Order Scheme for Thermally Driven Flows in an Open Channel, Computers and Fluids, 27:273-290, 1998

93. G. Kravchenko and P. Moin, On the Effect of Numerical Errors in Large Eddy Simulations of Turbulent Flows, J. Computational Physics, 131:310-322, 1997

94. P. Moin and K. Mahesh, Direct Numerical Simulation: A Tool in Turbulence Research, Annu. Rev. Fluid Mech., 30:539-578, 1998

95. H. L. Stone, Iterative Solution of Implicit Approximations of Multidimensional Partial Differential Equations, SIAM J. Numer. Anal., 5:530-558, Sept., 1968

96. D. W. Peaceman and H. H. Rachford, JR., The Numerical Solution of Parabolic and Elliptic Differential Equations, J. Soc. Indust. Appl. Math., 3:28-41, 1955

97. R. I. Issa, Solution of the Implicitly Discretised Fluid Flow Equations by Operator-Splitting, J. Computational Physics, 62:40-65, 1985

98. R. I. Issa, A. D. Gosman and A. P. Watkins, The Computation of Compressible and Incompressible Recirculating Flows by a Non-iterative Implicit Scheme, J. Computational Physics, 62:66-82, 1986

99. C. N. Rhie and W. L. Chow, Numerical Study of the Turbulent Flow Past an Airfoil with Trainling Edge Separation, AIAA Journal, pp.1525-1532, 1983

10. APPENDED PAPERS

1. Zhenghua Yan and Göran Holmstedt, CFD and Experimental Studies of Room Fire Growth on Wall Lining Materials, Fire Safety Journal, 27:201-238, 1996

2. Zhenghua Yan and Göran Holmstedt, Fast, Narrow-band Computer Model for Radiation Calculations, Numerical Heat Transfer, Part B: Fundamentals, 31:61-71, 1997

3. Zhenghua Yan and Göran Holmstedt, CFD Simulation of Upward Flame Spread over Fuel Surface, Proceeding of the 5th International Symp. on Fire Safety Science, pp. 345-356, 1997

4. Zhenghua Yan and Göran Holmstedt, Three-dimensional Computation of Heat Transfer from Flames between Vertical Parallel Walls, Combustion and Flame, in press

5. Zhenghua Yan and Göran Holmstedt, A Two-Equation Turbulence Model and Its Application to a Buoyant Diffusion Flame, International J. of Heat and Mass Transfer, 42:1305-1315, 1999

6. Zhenghua Yan and Göran Holmstedt, Numerical Investigations of Rack Storage Fires, submitted to the 6th International Symp. on Fire Safety Science

7. J. L. de Ris and Zhenghua Yan, Modeling Ignition and Pyrolysis of Charring Fuels, Proceedings of the 5th International Conference on Fire and Materials '98, San Antonio, TX, USA, pp. 111-121, 1998

(Note: The manuscript of this paper was prepared and submitted to the conference by the first author of this paper. The second author (Zhenghua Yan) may not fully agree on the content of this paper. Particularly, the reference to the second author's original work needs to be corrected. The pyrolysis model was origionally developed in the first paper appended in this thesis)